MULTIPURPOSE ASTROPHYSICAL ORBITAL OBSERVATORY "INCA" for direct study of high-energy primary cosmic rays

January 10, 2006

V.V. Ammosov[1], G.I. Britvich[1], N.Burtebaev[2], A.P. Chubenko[3], P.A. Chubenko[3], V.I. Drobzhev[4], V.F. Grishchenko[5], G.I. Kol'tsov[6], O.N. Kryakunova[4], S.V. Kryukov[4], G.I. Merzon[3], K.M. Mukashev[7], R.A. Mukhamedshin[8], V.N. Murashev[6], V.V.Oskomov[9], M.I. Panasyuk[10], V.P. Pavlyuchenko[3], S.A. Petrochenkov[11], D.M. Podorozhny[10], V.A. Ryabov[3], O.G. Ryazhskaya[8], T.Kh. Sadykov[12], T. Saito[13], A.L. Shchepetov[3], N.M. Sobolevskii[8], A.P. Soldatov[1], U.M. Sultangazin[5], B.T. Suymenbaev[5], L.G. Tkachev[11], V.G. Vasil'chenko[1], I.V. Yashin[10], G.T. Zatsepin[8], and A.P. Zhukov[8]

[1] Institute for High-Energy Physics, Protvino, Russia
[2] Institute of Nuclear Physics, Almaty, Kazakhstan Republic
[3] Lebedev Physical Institute, Moscow, Russia
[4] Ionosphere Institute, Almaty, Kazakhstan Republic
[5] Institute for Space Research, Almaty, Kazakhstan Republic
[6] Moscow State Institute of Steel and Alloys, Moscow, Russia
[7] Abai Almaty State University, Almaty, Kazakhstan Republic
[8] Institute for Nuclear Research, Moscow, Russia
[9] Al-Faraby Kazakh National University, Almaty, Kazakhstan Republic
[10] Skobel'tsyn Institute of Nuclear Physics, Moscow, Russia
[11] Joint Institute for Nuclear Research, Dubna, Russia
[12] Physical-Technnical Institute, Almaty, Kazakhstan Republic
[13] Institute for Cosmic Ray Research, University of Tokyo, Japan

Correspondence to: R.A. Mukhamedshin (muhamed@sci.lebedev.ru)

Abstract

A project of the unique multipurpose astrophysical orbital observatory "INCA" for direct study of spectra and composition of high-energy primary cosmic radiation in the range $10^{12} - 10^{16}$ eV based on the use of ionization-neutron calorimeter (INCA) as well as new technologies of particle detection is considered. Scientific goals of the MAOO "INCA" are discussed: (a) measurements of the PCR charge composition and energy spectra of different components in a wide range from several TeV up to the "knee" energies ($10^{15} - 10^{16}$ eV); (b) spectra of high-energy electrons and γ-rays; (c) search for γ-ray discrete sources and dark matter signatures; (d) neutral radiation from solar flares; (e) study of interactions of high-energy cosmic-ray particles and search for exotic particles.

Contents

1 Astrophysical and physical goals

1.1 Introduction

The goal of the INCA project is designing a multipurpose astrophysical orbital observatory (MAOO) "INCA" being sufficiently perspective to carry out fundamental studies in astrophysics of primary cosmic radiation (PCR) and physics of elementary particles at high energies ($E_0 \sim 10^{12} - 10^{16}$ eV) during the first quarter of the 21st century. It is planned to carry out

• measurements of spectra and charge composition of PCR components and estimation of their mass composition starting with $E_0 \sim 10^{12}$ eV right up to $E_0 \sim 10^{16}$ eV;

• measurements of the primary electron spectrum at $E_e \sim 10^{11} - 10^{13}$ eV;

• measurements of the spectrum of diffusive γ-radiation and search for discrete sources of γ-rays at $E_\gamma \sim 3 \cdot 10^{10} - 10^{13}$ eV;

• measurements of fluxes of neutrons and γ-rays from solar flares;

• estimation of the upper limit of the intensity of very massive exotic particles with $Z/m \ll 1$;

• estimation of the upper limit of cross section of strong interactions with unusual feature (interactions with abnormally high hadron-to-γ-ray ratio and/or neutron yield, etc.);

• measurement of the energy behaviour of particle-production cross section of protons and light nuclei up to $E_0 \sim 10^{15}$ eV.

For the first time in space experiments, it is proposed to apply the detection of both the ionization and neutron signals to measure energy of high-energy cascades. This makes it possible, on the one hand, to improve the accuracy of cascade energy measurement (Sect. 3.1) and separation of electrons against the background (Sect. 3.2), and, on the other hand, to pick out cascades with non-typical development initiated by exotic particles or interactions (Sect. 3.3).

1.2 Composition and energy spectrum of PCR in the "knee" range

One of the most important astrophysical problems is the study of the PCR energy spectrum with a near featureless shape obeying the power law extended for more than 11 orders of magnitude in energy and 30 orders of magnitude in intensity (Fig. 1) and giving an information on different processes taking place, on one hand, in cosmic ray sources (supenovae, pulsars etc. including, possibly, hypothetical superheavy particles), and, on the second hand, in the interstellar space in our Galaxy and intergalactic space. One of the most interesting questions is the nature of the sharp break ("knee") – the spectrum steepening [2] in the energy range $E_0 \sim 10^{15} - 10^{16}$ eV, i.e., the increase of the index of the summary differential spectrum of protons and nuclei from ~ 2.7 to $\sim 3.0 - 3.2$ at particle energies $E_0 > E_k \sim 3 \cdot 10^{15}$ eV (Fig. 2).

The "knee" nature could be related to both astrophysical origins and features of particle interactions. The "knee" is interpreted, in part, in terms of the galactic modulation [2, 3, 4, 5], i.e., of increasing inability of the galactic magnetic field to trap the particles. Other mechanisms have also been suggested, including photonuclear fragmentation of heavy nuclei in the vicinity of PCR sources [6, 7], terminated acceleration in supernova remnants [8, 9], contribution of extragalactic protons generated in AGN cores [10], and even a change in high energy interaction

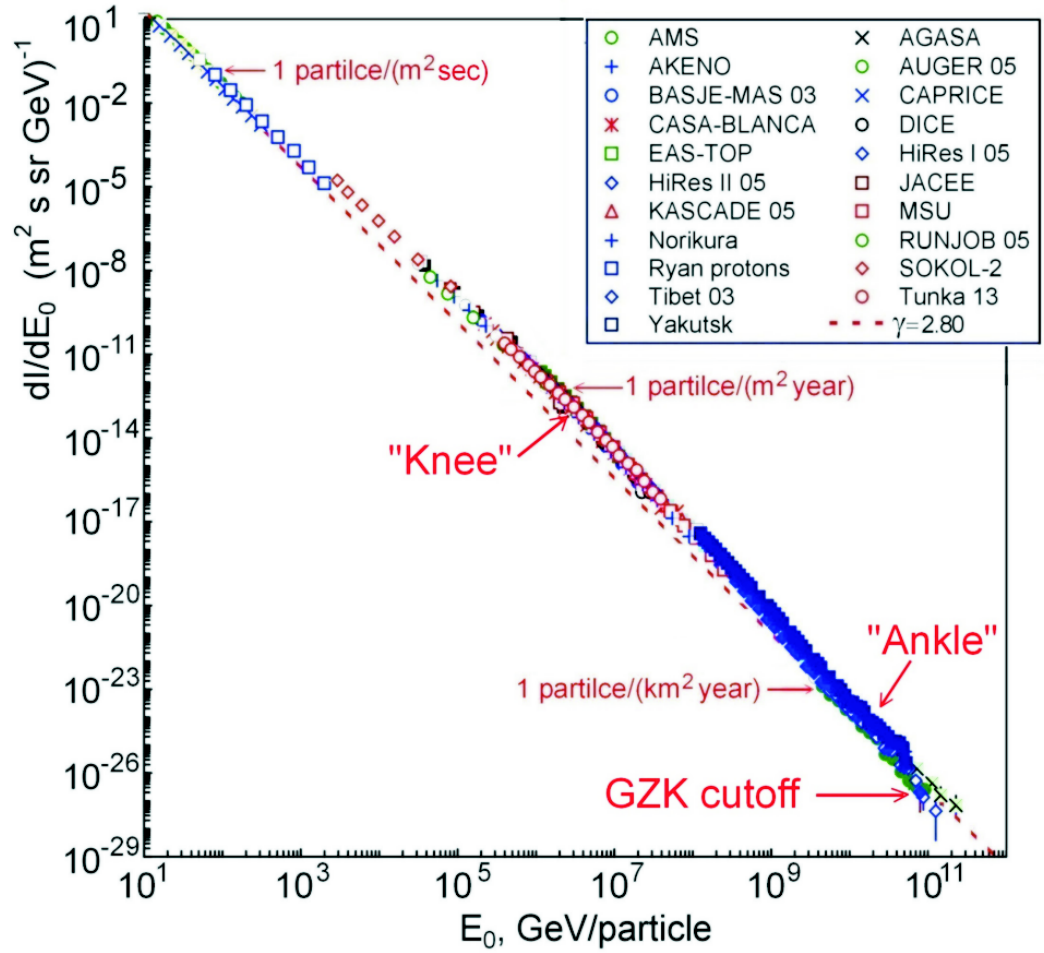

Figure 1: All-particle energy spectrum.

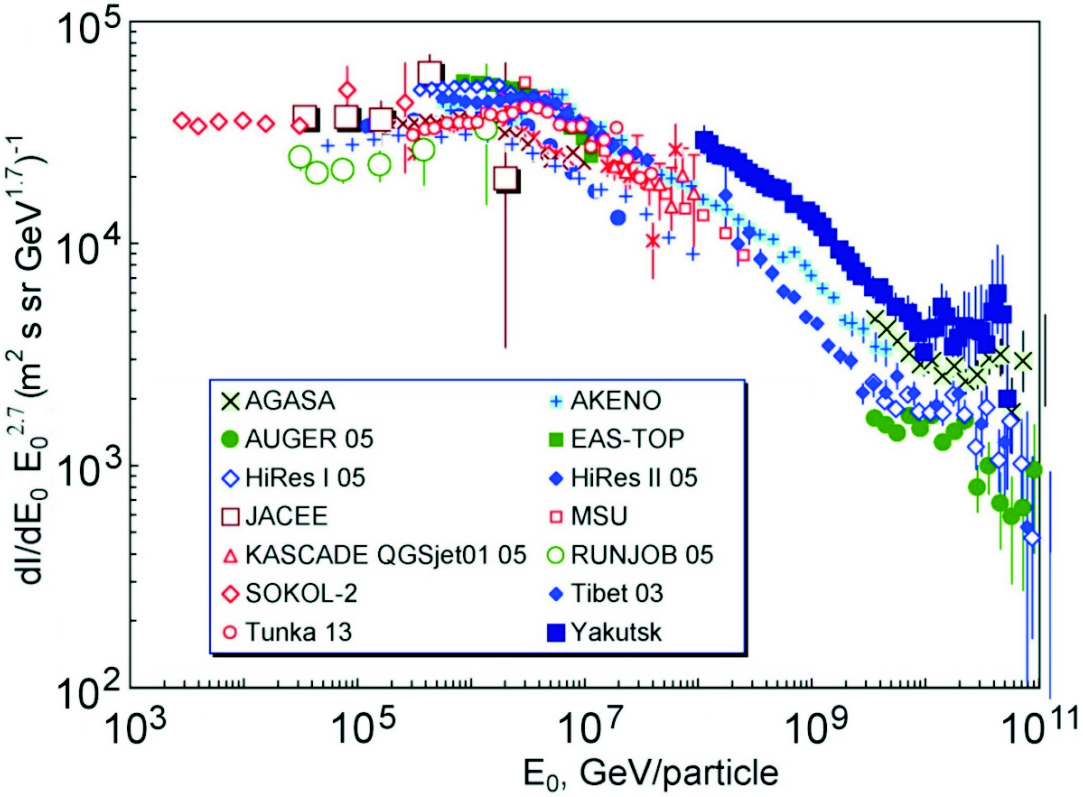

Figure 2: The "knee" range of the primary cosmic radiation spectrum.

characteristics in this energy region [11, 12, 13]. The variety of theoretical models is related to both the poor information on this range and the ambiguity of the available data. In almost all the models of astrophysical origin, the observed spectral shape was attributed to many cosmic ray sources. It was found [14, 15, 16] that the "knee" has a more complicated structure than a simple steepening with a rapid increase of the slope. Shower size spectra, measured in different experiments at various atmosphere altitudes have a few common features.

The first is that the "knee" is rather sharp and its sharpness cannot be reconciled with its origin from many cosmic ray sources or Galactic modulation. The second is that there is an evident intensity peak in the spectra at energies higher by a factor of about 4 than the energy of the "knee". These features have been interpreted as an evident contribution of the cosmic rays from just the single source, namely, a relatively nearby explosion of a supernova, for instance, Monogem, Loop-1, Vela, or Geminga [17, 18]. Based on the most recent model of the cosmic ray acceleration in such supernovae [9], the knee itself and the second peak in the spectrum have been interpreted as the contribution from primary oxygen and iron nuclei, respectively. In this case, the contribution of the youngest of them (Vela) is expected to be most important in the "knee" range, as well as in the electron spectrum at $E_e \gtrsim 10^{12}$ eV, although this conclusion depends on time of cosmic ray confinement in the supernova remnant [19].

The mass and isotope composition of PCR components could provide a very important information on origin and diffusion of cosmic rays. However, direct experimental data on mass and isotope composition at sufficiently high energies ($E_0 \gtrsim 10^{14}$ eV) are generally absent so far. All the data in the "knee" range are indirect and accumulated by observing secondary components of nuclear-electromagnetic cascades (NEC) in the atmosphere (EAS low-energy particles, γ-ray$-$hadron families, bundles of high-energy muons, Cherenkov radiation).

As a result, data by different experiments are often contradict one to another. Furthermore, even data of a single experiment (KASCADE, e.g.) could be in significant contrast. For instance, the dispersion of derived data on average mass of primary particles in the "knee" range are scattered from a mean between protons and helium nuclei in CASA-BLANKA and CASA-DICE experiments to magnesium nuclei in BASJE experiment. Data on energy dependence of proton-to-all particle spectrum ratio at $E_0 \sim 2 \cdot 10^{15}$ eV by KASCADE [21] and TIBET [22] experiments differ by a factor of ~ 2.5. The KASCADE's main conclusion is that the "knee" is determined by a very strong steepening ($\Delta\gamma \gtrsim 2$) of the proton spectrum at $E_0 \sim 2 \cdot 10^{15}$ eV, while heavier nuclei become extinct abruptly as well in accordance with their charge, determining integrally a more smooth steepening of the all-particle spectrum. The TIBET's conclusion is absolutely contrary and means that the smooth steepening of the proton spectrum begins at lower energies ($E_0 \sim 2 \cdot 10^{14}$ eV), while the "knee" is determined by the iron spectrum steepening. Obviously, these points of view are contrary and imply very different physics of processes occurring in the space. These results are derived by comparing ground-based array data with results of EAS calculations, which are strongly model-dependent. As a result, as is seen in Fig. 2, the dispersion of results is comparable with statistical errors of balloon experiments. However, the problem of choice of the "true" model seems to be practically unsolvable in the nearest future. So, direct measurements in the "knee" range with improved

Table 1: Parameters of fitted PCR spectra at $E_0 = 1000$ GeV.

Particle	p	He	Li	C	O	Mg	Si	V	Fe
$10^5 \cdot dI_{0i}/dE_0$ $(\mathrm{m}^2\ \mathrm{s\ sr\ GeV})^{-1}$	8.73	5.71	0.2554	1.267	1.950	1.164	1.223	0.6791	2.04
"KASCADE" spectrum									
γ_i	2.71	2.64	2.54	2.70	2.70	2.64	2.70	2.63	2.59
"TIBET" spectrum									
γ_i	2.74	2.75	2.54	2.70	2.70	2.64	2.70	2.63	2.59

resolution in energy and mass are necessary not only for the clarification of nature of cosmic ray origin by comparing new experimental data and specific predictions of modern theories but also for obtaining the information on features of particle interactions, and thereupon to make ground-based array data more accurate at higher energies of PCR particles.

As an consensus of opinion on the composition and form of spectra of PCR particles in the "knee" range is absent, to illustrate results expected for INCA we use below the expression

$$dI_{0\,\mathrm{tot}}/dE_0 = \sum_{i=1}^{9} dI_{0\,i}/dE_0 = \sum_{i=1}^{9} I_{0\,i}\, E_0^{-\gamma_i} (1 + [E_0/(Z \cdot E_b)]^2)^{-0.5\Delta\gamma_i} \qquad (1)$$

to fit two PCR-spectrum versions proposed by the KASCADE [21] and TIBET [22] experiments, which differ, first of all, in proton and He nuclei spectra. Table 1 lists component intensities, $dI_{0\,i}/dE_0$, at $E_0 = 1$ TeV [23] and magnitudes of indices of differential spectra, γ, applied in both the cases conventionally called "KASCADE" and "TIBET" versions. In doing so, $\Delta\gamma = 2.1$ and 0.4; $E_b = 3 \cdot 10^6$ and 10^5 GeV for "KASCADE" and "TIBET" fits, respectively.

In Sect. 2, two INCA versions (*I* and *II*) with different efficiency of $e^{\pm}$ and γ-ray detection are considered and compared (Table 2). However, below results obtained for the version *I* are mainly discussed. It should be noted only that the lower geometric factor of the version *II* will result in a relative increase of statistical errors by a factor of $\sim 10\%$.

Figure 3 displays data on protons, helium and iron nuclei spectra expected for INCA in the "knee" range for "KASCADE" and "TIBET" versions of the PCR spectrum for the exposition time $T_{\mathrm{exp}} = 3$ years and effective geometrical factor $\Gamma_{\mathrm{eff}} = 20$ m^{2}sr (see Sect. 3.4). Figures 4 and 5 demonstrate, respectively, results on energy dependence of proton-to-all particle spectrum ratio and mean mass number, $\langle \ln A \rangle$, expected for INCA for both the versions of the PCR spectrum. Results of direct RUNJOB and JACEE experiments as well as some data derived from ground-based EAS experiments are also shown. One could hope that INCA will make it possible to finish at last the discussion on the "knee" features.

For the exposition time $T_{\mathrm{exp}} = 3$ years and effective geometrical factor $\Gamma_{\mathrm{eff}} = 20$ m^{2}sr, the number of PCR protons and nuclei arriving onto the instrument will be as large as $N(E_0 > 10^{15}\ ) \simeq 2000$ and $N(E_0 > 10^{16}\ ) \simeq 30$. This statistics seems to be sufficient to resolve the main goals of the project and to clear important problems related to cosmic-ray local sources.

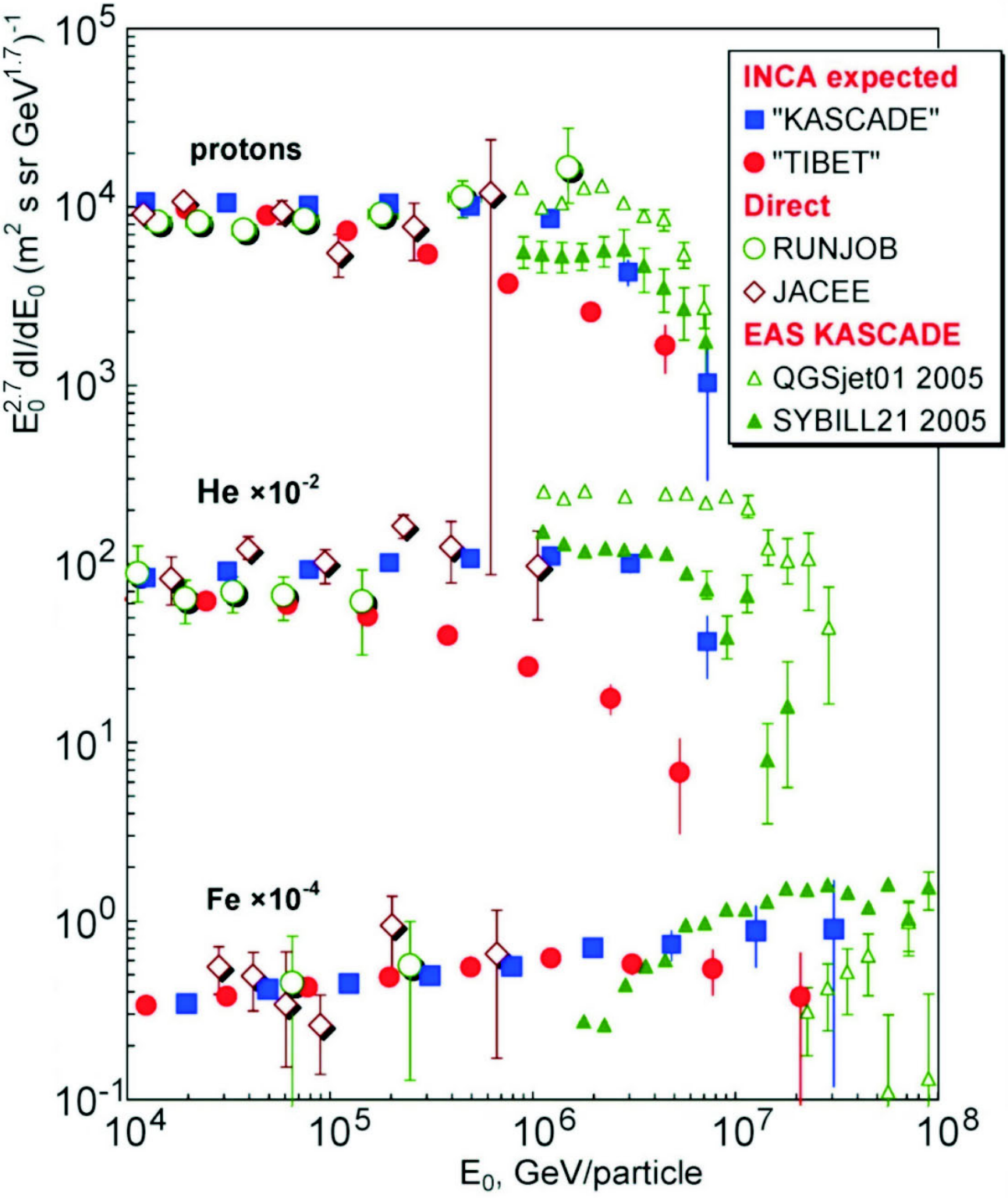

Figure 3: Data on spectra of protons, helium and iron nuclei expected for INCA for "KASCADE" and "TIBET" versions of the PCR spectrum.

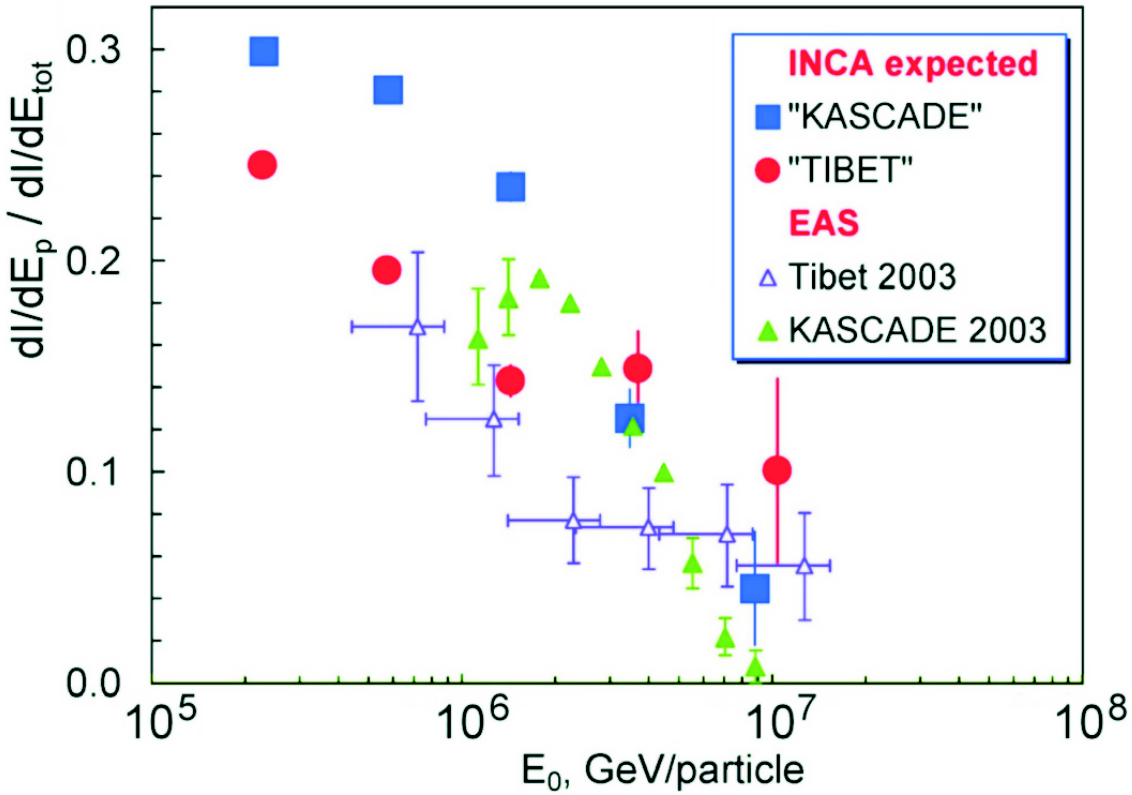

Figure 4: Energy dependence of proton-to-all particle spectrum ratio in the "knee" range by KASCADE and TIBET experiments and expected one for INCA for "KASCADE" and "TIBET" versions of the PCR spectrum.

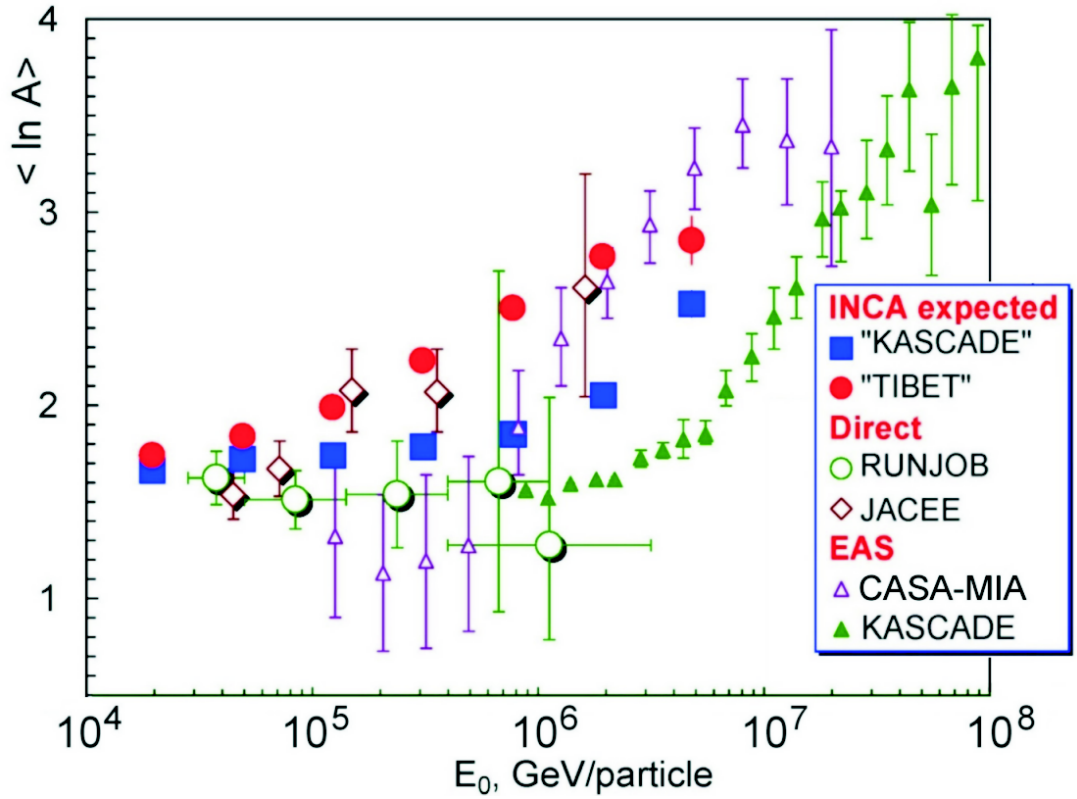

Figure 5: Results on mean mass number, $\langle \ln A \rangle$, expected for INCA for "KASCADE" and "TIBET" versions of the PCR spectrum. KASCADE and CASA-MIA data are shown as well.

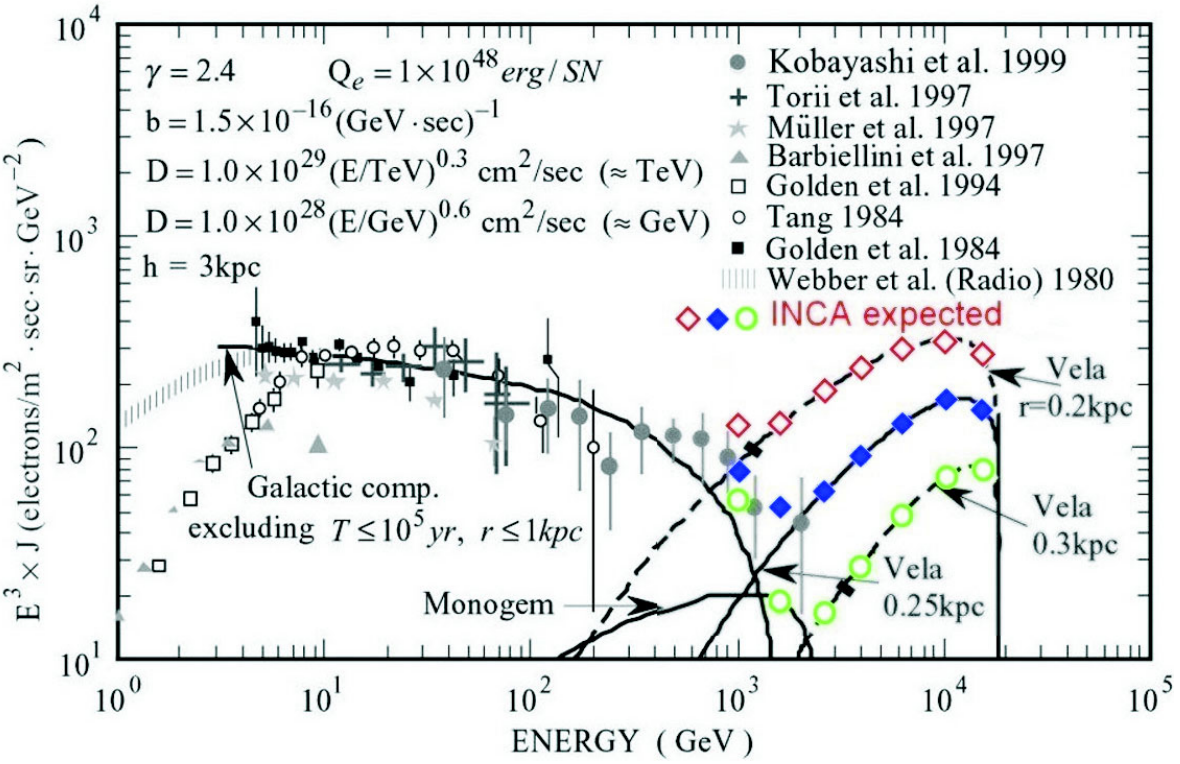

Figure 6: Cosmic ray electron spectrum [26]. Curves display calculated contributions of Monogem and Vela for different distances. Symbols on these curves show data expected for INCA.

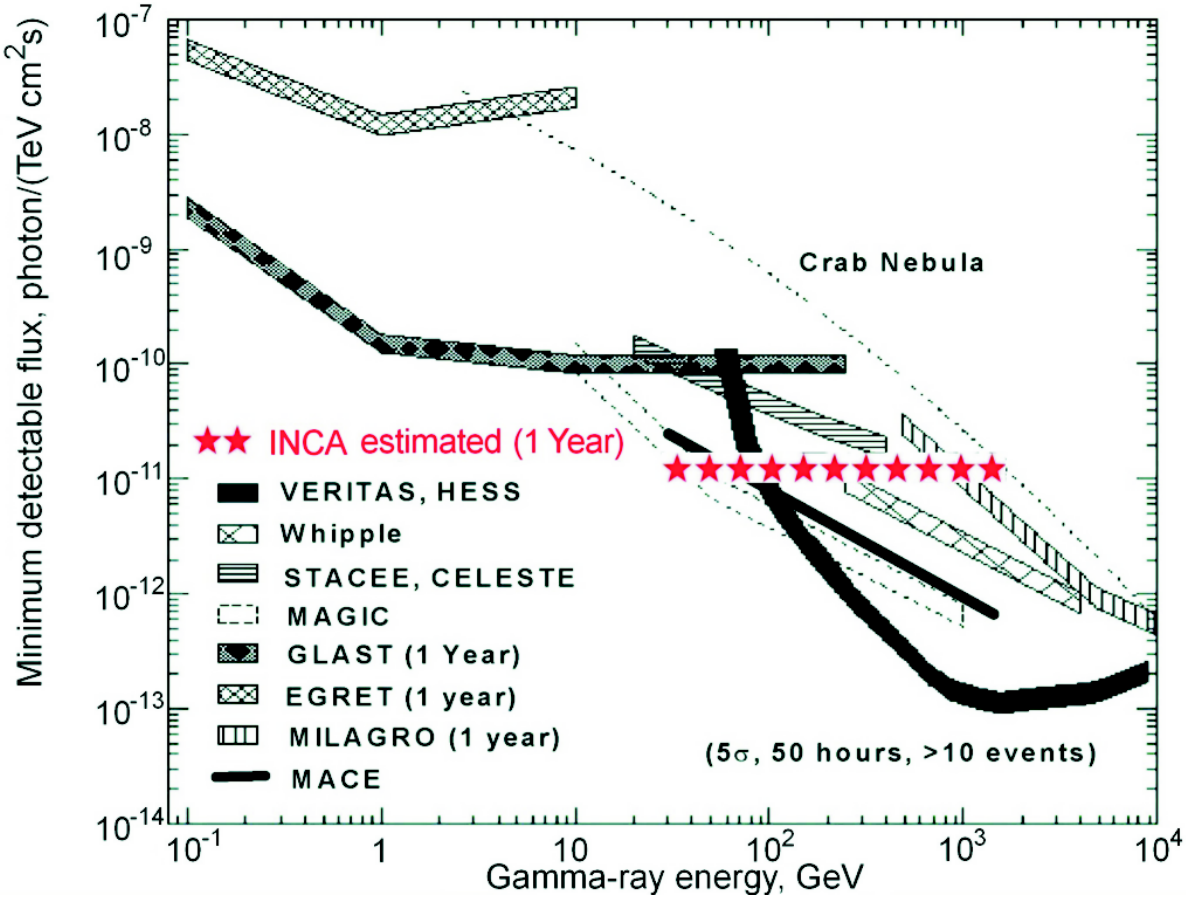

Figure 7: Minimum detectable flux of γ-rays in different arrays and instruments [42].

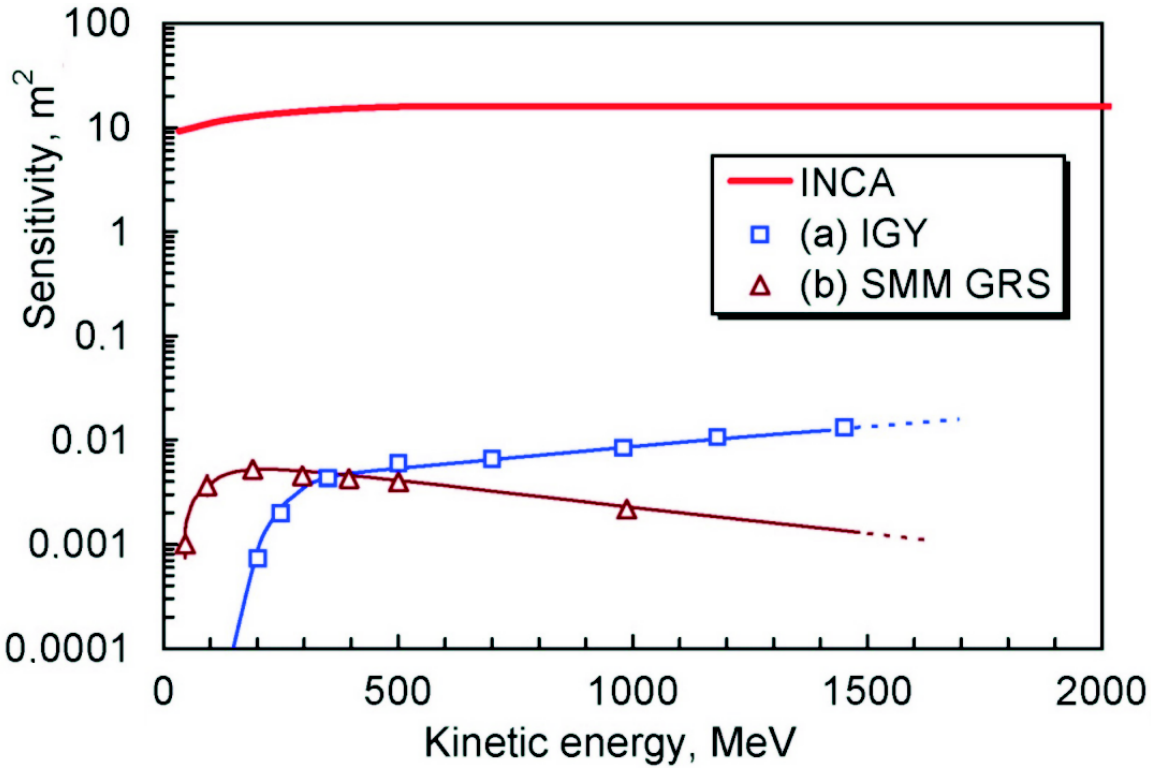

Figure 8: Sensitivity functions of INCA, SMM GRS, and a standard IGY neutron monitor at 498.0 mm Hg atmosphere pressure for primary neutrons incident onto the top of the atmosphere.

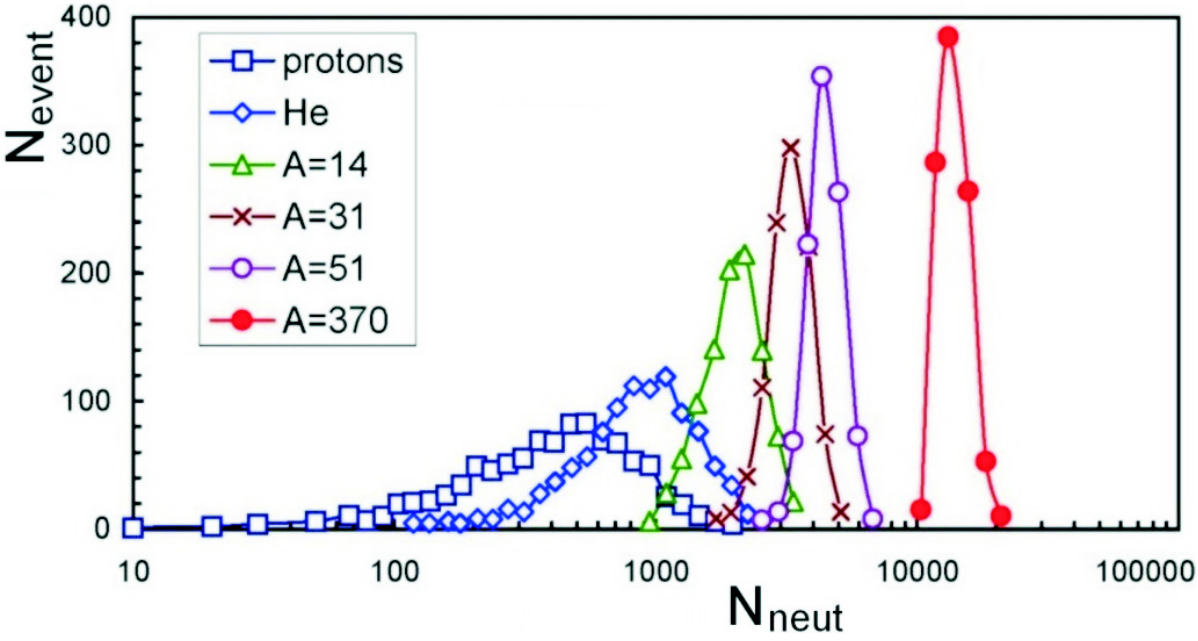

Figure 9: Neutron number distributions in INCA caused by primary nuclei ($A = 1, 4, 14, 31, 51$) at $E_0 = 1.0 - 1.78$ TeV. X-particles are assumed to interact as "superheavy nuclei" with $A = 370$.

1.3 Spectrum of electrons from nearby sources

The spectrum of electrons in the actually unexplored energy range $E_e \gtrsim 10^{12}$ eV could provide a very important information on nearest supernovae.

Electrons constitute only a small part ($\lesssim 1\%$) of the total PCR flux near the Earth. Nevertheless, their role in studying the Galaxy is very important. The reason is that electrons efficiently loose their energy due to ionization, bremmstrahlung, synchrotron radiation and inverse Compton scattering, thus being a sensitive probe for the interstellar matter and magnetic fields. The other aspect is that PCR electrons with very high energies ($E_e \gtrsim 10^{12}$ eV) are expected to come only from a few nearby sources [17, 18, 25] and the age of the observed TeV electrons cannot significantly exceed 10^5 yr.

It implies the existence of nearby supernova sources at a distance $R < \sqrt{2D\,t} \simeq 500$ pc. The most obvious candidates for such sources are supernovae. The occurrence of supernovae in the Galaxy is assumed to be at a rate of one per $30-100$ years. For 1-TeV electrons, within their propagation domain of about 300 pc from the solar system, the expected number of supernova occurrence is only $2-5$ during the past $3\cdot10^5$ years [25, 27]. Only these few sources (most likely, the most young supernova Vela) could contribute efficiently to the electron flux at $E_e \gtrsim 10^{12}$ eV. The measured intensity from each of the sources (Vela, e.g.) depends on source distance (Fig. 6 [26]) as well as the time of cosmic ray confinement in the supernova shell. If it is as large as $0.5\cdot10^5$ years, the main contribution into the high-energy electron intensity is produced by Monogem and Cygnus Loop [31].

Thus, measurements of the high-energy electron spectrum at $E_e \gtrsim 10^{12}$ eV can resolve fundamental issues of the most important PCR acceleration mechanism and of the role of nearby local sources.

First in space studies, the INCA project proposes to apply a new technique of separation of electron-produced cascades from the proton-produced background (see Sect. 3.2).

Figure 6 displays results on electron spectrum measurements expected for INCA. It is expected that during the exposition time $T_{\rm exp} = 3$ years and effective geometrical factor $\Gamma_{\rm eff} = 20$ m^{2}sr, the number of PCR electrons arriving onto the instrument will be as large as $N(E_e > 10^{12}\ \text{eV}) \gtrsim 2\cdot10^4$ or more due to the detection of Vela-generated electrons.

1.4 High-energy gamma rays in space

Independence of electric and magnetic fields and low absorptqon in interstellar and intergalactic space makes the cosmic γ-radiation a unique tool for investigation of astrophysical objects. Experimental data are now available at $E_\gamma < 30$ GeV (satellites and balloons) and at $E_\gamma \gtrsim 300$ GeV (EAS arrays).

In the high-energy region ($E_\gamma < 30$ GeV), galactic discrete γ-ray sources (pulsars) and extragalactic sources (active galactic nuclei) were detected at a high confidence level. For the most intense of them (Vela, Crab, and Geminga), the energy spectra were obtained and models for generation mechanisms were proposed. In the region of the superhigh energies ($E_\gamma \gtrsim 1$ TeV), γ-ray emissions from the Crab nebula and the extragalactic objects Mk421, Mrk501, and

1ES2344+314 were reliably detected.

At the same time, data from discrete γ-ray sources in the intermediate energy range $30 \lesssim E_\gamma \lesssim 1000$ GeV, which could be very significant for resolution of some important problems, are rather poor. To understand the nature of these sources, we need to know the shape of the energy spectrum in detail. The available data show that in most cases it has significantly different spectral index in two mentioned energy ranges. For instance, the integral spectral indices for Vela and Geminga vary from 1.89 [27] to 3.5 [35] and from 1.8 [36] to 2.3 [38], respectively. The recent theoretical models [38, 39, 40] failed to explain the entire γ-ray spectrum of pulsars from tens of MeV to hundreds of TeV. As soon as the changes of the spectral index are expected in the energy range $30 \lesssim E_\gamma \lesssim 1000$ GeV, relevant investigation will present an unique information for understanding the processes that occur in the astrophysical objects known as γ-ray sources. Direct measurements of the γ-ray spectra from discrete sources in the energy range under consideration will also provide a calibration method for indirect ground-based measurements, thus significantly increasing their reliability.

The diffuse γ-radiation in the Galaxy at $E_\gamma > n \cdot 100$ MeV is thought to arise from decay of π^0 mesons produced as a result of interactions of cosmic ray protons and nuclei with the interstellar matter. The resulting γ-ray energy spectrum is expected to be similar to the proton spectrum. However, the spectrum of γ-rays from the galactic disk in the internal galaxy region extracted from COS-B [41] and EGRET [34] data up to energies of 30 GeV is flatter than the local cosmic ray spectrum. This experimental result could be explained by the contribution of either unidentified γ-ray sources with a flat spectrum or γ-rays generated in the inverse Compton effect process, or by more hard PCR spectrum in the internal galaxy region. The investigation of the spectrum shape in the higher energy range (up to 1 TeV) makes it possible to clarify the relation between the contributions of PCR protons and electrons into the γ-ray generation and to reconstruct the high-energy electron flux using the measured γ-ray spectrum, thus cross-checking the results of the direct measurements of the electron spectrum.

Thus, INCA measurements with a large geometrical factor ($\sim$ 20 m^2·sr), high angular resolution ($\sim 1'$), exposure time of 3 year (or more), and an γ-ray-energy measurement accuracy of several percent (version *II*), could give an important information on cosmic γ-radiation in general as well as make it possible in particular to search for dark-matter signatures produced, for instance, through the neutralino annihilation, in a wide range from $\sim$ 30 GeV up to TeV energies. Figure 7 [42] indicates that INCA is comparable in sensitivity with the majority of ground-based arrays designed for γ-ray detection.

1.5 Neutral radiation from solar flares

High-energy phenomena on the surface of the Sun are manifestations of a part of the solar dynamo cycle. The dissipation of energy followed by an intense heating and acceleration leads to the emission of X-rays and fast particles. These particles, in turn, give rise to hard X-rays, γ-rays, neutrons, and solar cosmic rays. In high- energy astrophysics, such phenomena are expected to occur in accretion disks around such compact objects as black holes and in

quasars. The majority of such phenomena is not yet completely investigated. In particular, the relationship between charged particles and neutral radiation (γ-rays and neutrons) is still obscure because of trapping of charged particles in solar magnetic fields and probable contribution of interplanetary acceleration. From experimental data on γ-rays and neutrons, which are not deviated or trapped by magnetic fields and therefore give a direct information about acceleration site and temporal characteristics, one can derive the following information [44]: (1) a fraction of released energy which is converted into high-energy particles; (2) an absolute number of accelerated particles; (3) a shape of energy spectrum and upper limit of the energy of accelerated particles; (4) a rate and duration of particle acceleration; (5) features of mechanisms of particle acceleration which incorporate all characteristics mentioned above; (6) conditions in the ambient solar plasma wherein these mechanisms are realized.

In a number of events, solar neutrons of several hundreds megaelectronvolts have been detected by neutron monitors at mountain altitudes. However, the neutron monitor sensitivity to solar neutrons is limited and still rather controversial due to indirect character of the observations. That is why the first solar neutrons have been recorded in the satellite experiment [45]. However, in both this and later (CGRO) experiments, γ-ray detectors with rather low geometry factors, which had not been specialized for neutron detection, were used. This resulted in low statistics and restricted the neutron energies by several hundreds MeV.

In fact, the INCA could be the first neutron monitor combined with the ionization calorimeter and operating outside the Earth's atmosphere, and give an unique opportunity to observe simultaneously solar γ-rays and neutrons with energies that may be indicative of the upper limit for the solar acceleration. This would be a precise information on fundamental problems of charged particle acceleration and transport.

The INCA capabilities for neutron detection are illustrated in Fig. 8, where sensitivities of the SSM GRS satellite detector and a standard mountain neutron monitor are compared to the expected INCA sensitivity, which turns out to be 2 to 3 orders of magnitude higher.

Statistical errors expected while recording solar flares by the INCA could be by about one order of magnitude lower than that for the SMM GRS detector. Such a high sensitivity allows us, despite of a high galactic PCR background ($\sim$ 1.5 kHz), to record solar flares with the neutron intensity of $\sim 10^{-2}$ cm^{-2}s^{-1} at a level of three standard deviations.

1.6 Search for exotic particles and study of interactions

The predominant part of the Universe mass is invisible. It is hidden in some non-luminous objects of unknown type and until now is detectable only through its gravitational effect on luminous matter. It is usually assumed that the dark matter (DM) consists of neutral particles (neutralinos, axions, massive neutrinos etc.) and interact with the ordinary matter only weakly. However, various kinds of massive particles interacting also electromagnetically and even strongly (so-called SIMPs) has been shown to be compatible with DM. These particles denoted as X could have a very large mass numbers $A = M_X/m_p \gg 1$, and an anomalously low ratio $Z/A \ll 1$ [46]-[48]. It is believed that a certain small part of such particles could be

accelerated up to high energies similarly to usual nuclei. Evidences for such fast exotic particles have been found in a balloon experiment [49] and, possibly, in LEP experiments on study of muon bundles of highest multiplicities related to the "knee" range [43]. High-energy X particles could be detected by INCA as superheavy nuclei with an abnormally low Z/A ratio. The charge of these exotic particles will be measured in a wide range of Z by the charge detector, while the values of A can be estimated by the use of INCA's capability to estimate roughly the baryon number of incoming particles. We assume the X particles to interact similarly to very massive nuclei; this is true, most likely, for strangelets). Fig. 9 shows approximate distributions over neutron number in an absorber 1 λ_{int} thick generated by different nuclei and illustrates qualitatively the ability of INCA of measuring the mass number A of a "superheavy nucleus".

Assuming the shape of high-energy X particle spectrum suggested in [49] to be valid, we could expect that $\sim 10^{-6}$ of particles detected by INCA will be exotic ones.

One cannot exclude that the phenomenon of so-called "Centauros" (interactions with abnormally high hadron-to-γ-ray ratio observed at mountain levels) is related to the above problem. Although it was assumed earlier that it is a result of specific interactions of protons with energies in the "knee" range, it is possible nowadays to study the astrophysical origin of this phenomenon, in particular, its explanation by a decay of high-energy strangelet [50]. Features of INCA will make it possible, at least, to estimate the upper limit of the cross section of "Centauro"-type interactions.

At last, a large interaction statistic ($N(E_0 > 10^{14})$ eV $\simeq 10^5$) will make it possible to study the distribution of interaction points of protons and light nuclei over INCA depth and to find the energy dependence of their cross sections up to $E_0 \lesssim 10^{15}$ eV.

2 Description of the INCA project

2.1 The INCA's principal novelty

MAOO "INCA" is an unique cosmic-ray detector based on the use of new technologies of elementary particle detection. The basically new approach in space studies of cosmic rays proposed in this project is

• the use of new type device – ionization-neutron calorimeter (INCA), being very promising for future experiments in different fields of astrophysical and cosmic-ray investigations;

• the use of a light substance (e.g., polyethylene) as the dominant one of the absorber that makes it possible to provide the maximum geometry factor unattainable by another techniques;

• the measurement of nuclear-electromagnetic cascade energy by two methods: by measuring the flow of charged particles and counting the yield of evaporated neutrons in the ionization-neutron calorimeter (see Sect. 3.1);

• the separation of primary electrons (γ-rays) from the proton-produced background by using the fact that the yield of evaporated neutrons is much lower in electromagnetic cascades that in hadron-initiated ones [51] (see Sect. 3.2).

First in direct space study of high-energy cosmic rays, the INCA project applies the following new technologies.

• scintillators made of pressed polyethylene with admixtures containing boron, cadmium, and gadolinium, and used as position-sensitive detectors of both neutron and ionization signals (see 2.3.1);

• vacuum photo triodes and plastic photo sensitive plates (see Sect. 2.3.3).

A basically new analogue-free technology is specially developed for this project, namely,

• charge coordinate-sensitive detectors on the basis of semiconductor matrix bipolar silicon structures with internal amplification (see Sect. 2.3.4)

A modification of technical elements of the total construction for solution of specific goals is possible. In part, two INCA versions (*I* and *II*)) with different efficiency of detection of electromagnetic particles, in part, γ-rays, are considered.

2.2 Main properties of INCA

Basic characteristics of two versions of the current INCA conception (below versions *I* and *II*) are schematically shown in Figs. 10 – 13 and listed in Tables 2 – 5. These versions differ mainly in thickness of the lead plates. All other variations are related to this fact.

A layout of INCA's version *I* is shown in Fig. 10. The interior calorimeter has 50 levels, each consisting of the lead and polyethylene layers with a thickness of 1 and 29 mm, respectively, and the layer of long ($L_{\rm cal} = 200$ cm) plastic scintillator logs with a thickness of 10 mm (Fig. 11). Each of the scintillation logs may include an wavelength shifter (fibers or strips) as well as plastic photosensitive plates mounted on surfaces of scintillator logs. Polyethylene and lead constitute ∼78% and 22% of the total weight. This is equivalent respectively to 4.3 and 0.3 in proton interaction paths, λ^p_{int}, or to 4 and 9 t_0 in radiation lengths.

Plastic scintillator logs are used as position-sensitive detectors of neutron and ionization signals (see Sect. 2.3.1). PMTs, photo-triodes, and avalanche diodes are used as photodetectors. At the ends of the 80% of scintillation strips, phototriodes are placed for registering the ionization component of developed cascades in the amplitude-measurement mode. Phototriodes are proof against intense light flows; their photo sensitivity depends rather weakly on voltage variation.

Three following ways of pulse-counting mode detection by scintillators of weak neutron-produced signals are possible: (1) light-guide wavelength shifter fibers passing through scintillators transmit neutron-produced single light pulses to avalanche diodes; (2) plastic photosensitive plates mounted on surfaces of scintillator logs.; (3) sensitive PMTs are placed at the ends of 20% of scintillator logs. In the mode of neutron component detection, scintillators will detect mainly signals caused by delaying γ-rays generated due to the neutron capture by Cd and Gd nuclei and going relatively far away from points of their origin. To detect just neutrons near the points of their generation, 100 SNM17 200-cm long gas neutron counters are placed inside the each fifth polyethylene layer at 20 cm intervals (Fig. 10).

The INCA's exterior consists of two layers (*A* and *B*) separated with a gap (Figs. 10 and 12). The layer *A* constitutes a 1-cm thick polyethylene layer containing a 1-mm thick charge detector (CD) (see Sect. 2.3.4) divided into 5.5×5.5 cm^2 sections and coated by a 3-mm thick polyethylene film. The layer *B* is made of 5-cm thick polyethylene; PMTs and phototriodes are coming through its openings. "Helium-2" neutron counters are placed inside this layer. The INCA's exterior linear dimension is $L_{\rm tot} = 220$ cm.

Figure 12 shows the INCA's section in the plane traversing through one of the SNM17 counters. Figure 13 demonstrates a side view of one scintillator block.

Table 2 lists main technical parameters as well as scientific and physical properties of the INCA setup versions *I* and *II* which could be changed in future to optimize the device construction.

Below the version *I* is mainly considered. The total mass and power consumption are determined in more detail by parameters given in Tables 3 and 4, respectively.

The number of registration channels with ADCs (16000) is determined by parameters given

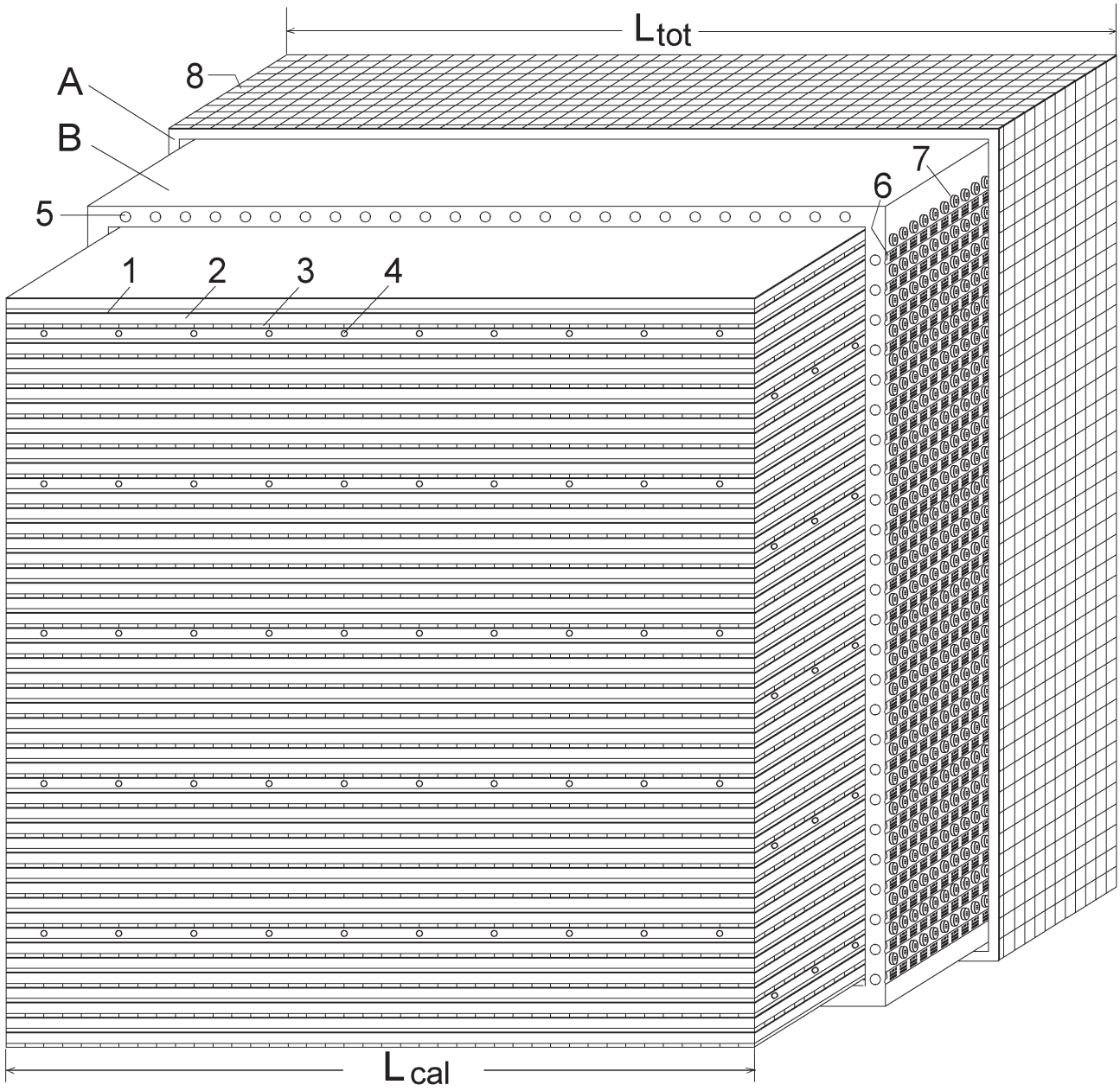

Figure 10: Layout of the ionization-neutron calorimeter and outer part of the device: (1) lead; (2) polyethylene ; (3) plastic scintillators; (4) SNM-17 gas detectors; (5) "Helium-2" gas detectors; (6) electronics boards; (7) photodetectors; (8) charge detectors. A and B are outward layers. $L_{\rm tot}$ and $L_{\rm cal}$ values are given in Table 2.

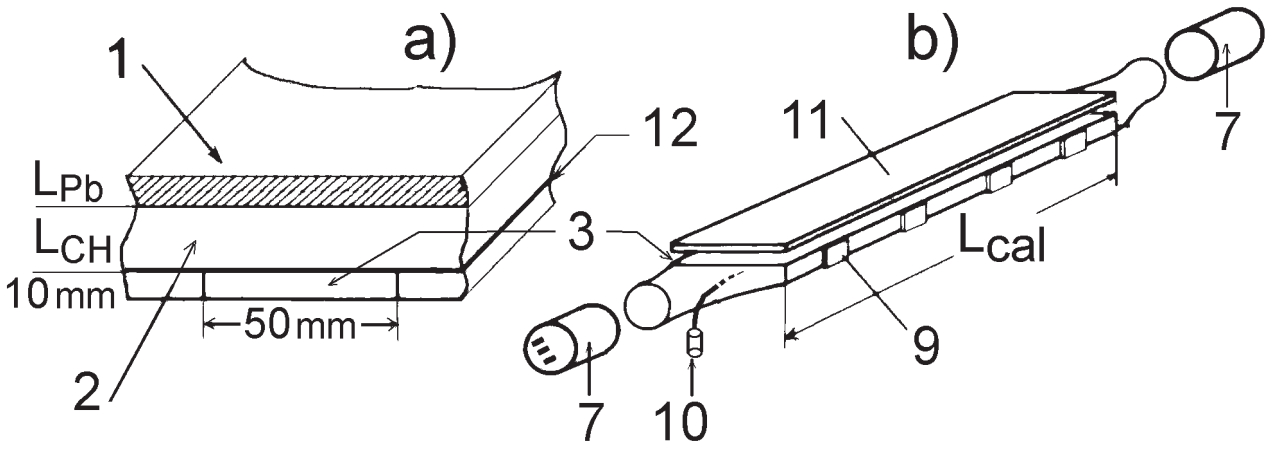

Figure 11: a) A part of section of one calorimeter layer; b) a layout of scintillation block. Notation (1) – (8) are the same as in Fig. 10; (9) photo plates; (10) fiber with avalanche photo diode; (11) wavelength-shifting light guide; (12) paint coat containing Cd or Gd foil maid of Cd or Gd. Proportions are not fulfilled. $L_{\rm Pb}$ and $L_{\rm CH}$ values are given in Table 2.

in Table 5. The number of channels for registration of neutron and gamma pulses (525) is determined by number of "Helium-2" neutron counters (1250) and scintillator detectors with avalanche photo diodes (APD) (400). The primary information content for one recorded event (51 KByte) is determined by parameters given in Table 5.

The total content of primary information registered at 5000-events/day trigger intensity is 255 Mb/day. If so, the content of compressed data message is 50 Mb/day.

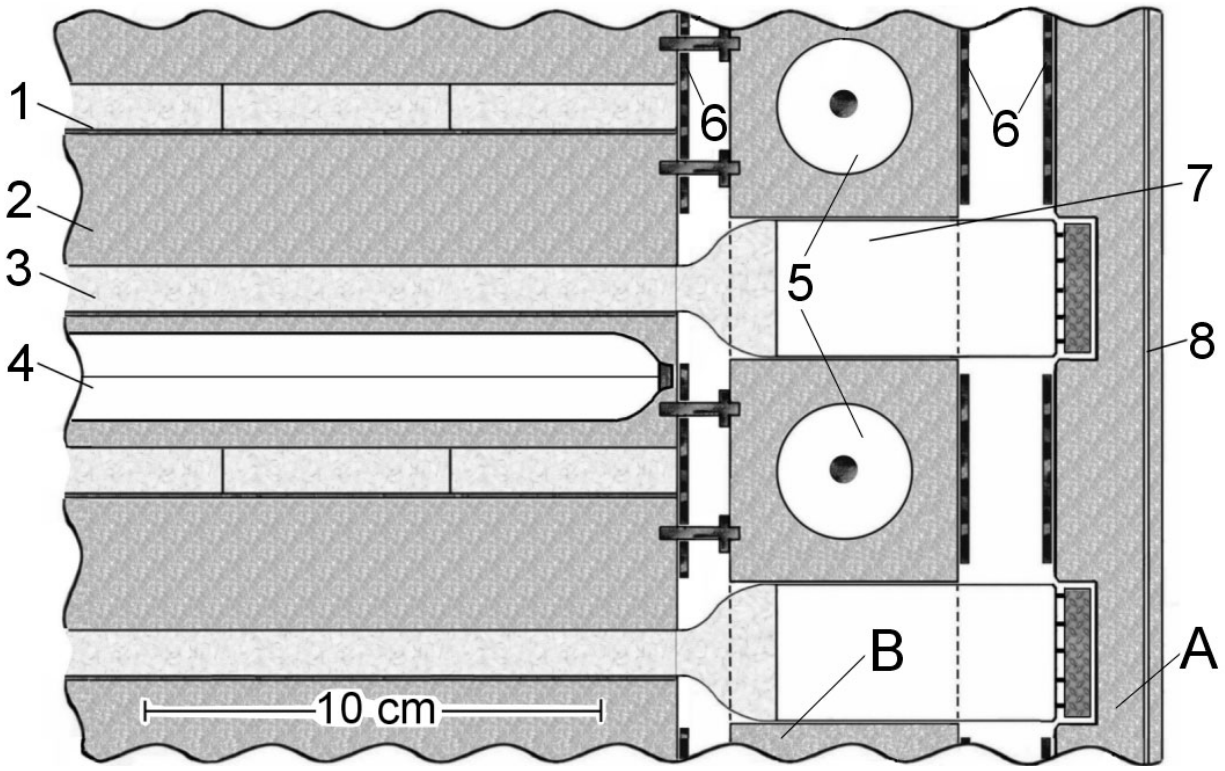

Figure 12: Section of the calorimeter and outer part of the device. Notations are the same as in Figs. 10 and 11.

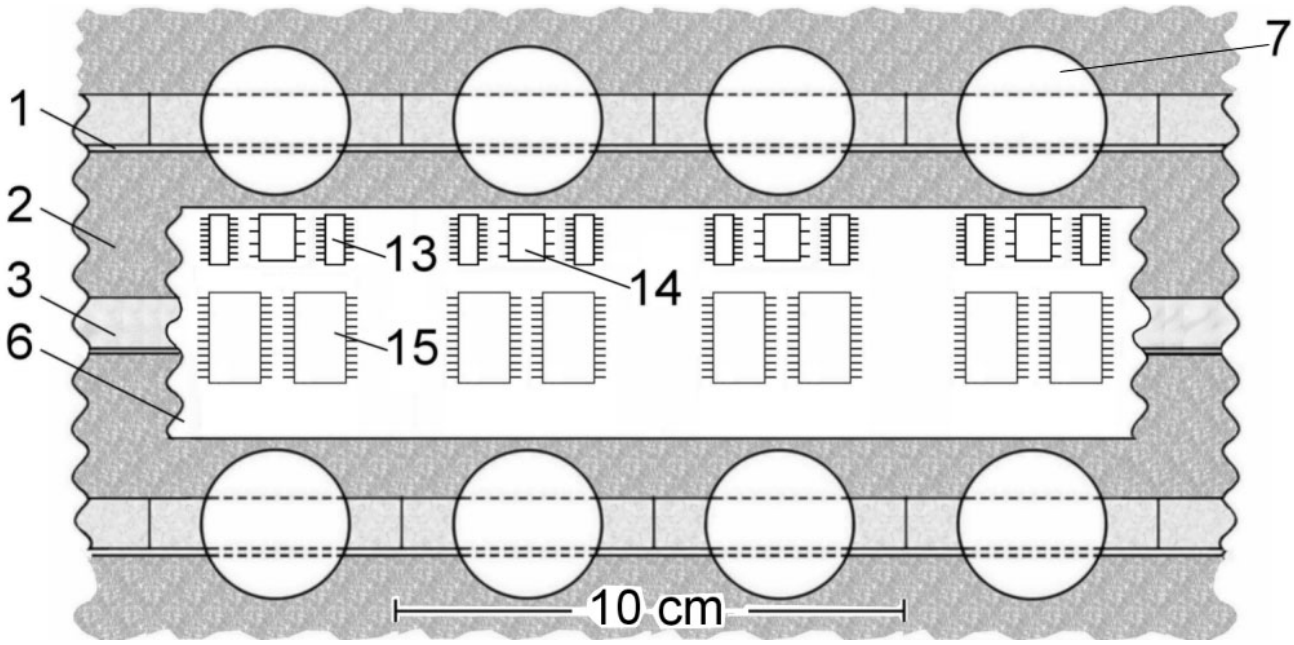

Figure 13: Possible side view of the calorimeter and an electronics board. Notations (1)– (12) are the same as in Figs. 10 and 11. (13) amplitude-digital converter AD7888AR; (14) operational amplifier 544UD2; 15) shifting register (CMOS-based serial-to-parallel code converter) 564IR13.

Table 2: Basic technical and scientific characteristics of cubic INCA versions (*I* and *II*).

Parameter	*I*	*II*
Total weight, kg	11050	11030
Calorimeter weight, kg	10000	9980
Linear total dimension, $L_{\rm tot}$, cm	220	208
Linear calorimeter dimension, $L_{\rm cal}$, cm	200	188
One-layer lead thickness, $L_{\rm Pb}$, cm	0.1	0.2
One-layer polyethylene thickness, $L_{\rm CH}$, cm	2.9	2.72
Thickness of the polyethylene reflector	5	5
Thickness of the charge detector's platform	1	1
Gaps between calorimeter, reflector, CD platform	4	4
Number of layers	50	48
Number of scintillators (5 cm$\times$1 cm$\times L_{\rm cal}$)	2000	2000
Number of photodetectors (PMT, phototriodes)	4000	4000
Number of avalanche photodiodes	400	400
Number of silicon detector plates (5.5×5.5 cm^2)	8000	8000
Number of ADC channels	16000	16000
Number of neutron- and γ-pulse counting channels	525	525
Power consumption, W	500	500
Primary information content per one registered event	51 kb	51 kb
Active life time of scientific equipment	$\geq$3 years	$\geq$3 years
Thickness in terms of		
proton's m.f.p. for interaction, $\lambda^p_{\rm int}$	4.6	4.5
radiation length, X_0	13	21
Device aperture	$\sim 2.7\ \pi$	$\sim 2.7\ \pi$
Geometric factor, m^{2}sr	~ 20	~ 17.6
Limit angular resolution	$\sim 1'$	$\sim 1'$

Table 3: Mass distribution of INCA (version *I*) components.

Component name	Mass, kg
Calorimeter (lead, polyethylene, and scintillators)	10000
Gaz-discharge neutron counters (120 pieces 0.5 kg each)	60
Phototriodes (4000 pieces 0.07 kg each)	280
Polyethylene shield-reflector	150
Silicon charge detector (CD) on polyethylene plate 1 cm thick)	500
Electronic registration channels, control and data acquisition systems	60
Total	11050

Table 4: Distribution of the INCA (version *I*) power consumption

Function	Voltage, V	Power, W
Stabilised power supply of phototriodes and neutron counters	2000	50
Stabilised power supply of the charge detector and avalanche photo diodes	100	10
Power supply of the calorimeter and charge detector registration channels	5	240
Control and data acquisition systems	–	100
Power reserve	–	100
Total		500

Table 5: Primary information content per one recorded event (version *I*) .

System	Channel number	Information content per channel	Additional requirements	Total, KByte
Calorimeter	8000	12 bit	2 ADC per phototriode	12
Charge detector	8000	12 bit	1 ADC per section (5.5×5.5 cm^2)	12
System of registration of delayed particles	525	1 byte	50 intervals per channel	26
Systems of monitoring and control	–	–	–	1
Total				51

2.3 Detectors

2.3.1 Scintillators

The detection of both the charged ionizing component and thermalized neutrons generated during the NEC development inside the instrument is of fundamental importance for the INCA project. However, the design of an effective large-dimension scintillator detector being able to detect signals caused by both the components is a nontrivial problem. This is related first to a relatively strong attenuation of the light signal at distances up to ~ 2 m. Besides, total multiplicities of neutrons generated and thermalized in the calorimeter volume could be as large as $\langle N_{neut} \rangle \gtrsim 10^6$, although differential (in coordinates and time) intensities would be significantly lower (Figs. 18 and 19). Mean times of thermalization and diffusion of thermalized neutrons before the capture in hydrogenous media are $\tau_{\rm therm} \lesssim 2\,\mu$s and $\tau_{\rm capt} \gtrsim 100\,\mu$s (Table 6). So, it is necessary to register neutron signals in a counting mode during a long time interval, $\tau_{meas} \lesssim 300\,\mu$s. On the other hand, the amplitude of each single signal is rather small, as neutron signals are distributed over a long time period. Besides, high rate of signal processing and time resolution $\Delta\tau_{res} \lesssim 10$ ns, are required.

The multiplicity of charged particles also achieves great values, $\langle N_{ch} \rangle \gtrsim 10^6$ (Fig 16) in the time $\tau_{ch} \sim 1\,\mu$s. This demands a wide ($\sim 10^7$) dynamical range from detectors.

The characteristic value of the lateral distribution of the charged component is $R_{\rm ch} \sim 10$ cm. The neutron distribution is more wide due to the thermalization process ($L_{\rm therm} \lesssim 10$ cm) and diffusion before the capture ($L_{\rm capt} \lesssim 10$ cm) (Table 6).

Intense signals produced by the ionizing component and used to determine the cascade axis become weaker at scintillator log ends. On the other hand, it is possible to measure one coordinate (along the strip axis) with an accuracy of $\delta_x \sim 2$ cm at the scintillator log length $L_{\rm log} = 200$ cm and scintillator's light attenuation length $\lambda_{\rm att}^{\rm sc} \sim 50$ cm.

Methods of detection of thermalized neutrons by using scintillators could be conventionally divided into two types: with and without localization of their generation points. It is desirable to use both these techniques to obtain a more full information on cascade development.

In the first case it is possible to use plastic scintillators containing ^{10}B. If so, products of ^{10}B(n,α)^{7}Li reaction are detected. In 94% of cases, this reaction occurs through the formation of 1.47-MeVα particles and excited state ^{7*}Li, which quickly transforms to the ground state (^{7}Li) with the 0.478-MeV γ-ray emission. At the present time, a polystyrene moulded scintillator SC-331 [52] is studied. It contains $2-3\%$ of the natural boron with a light yield of $56-60\%$ of that of anthracene, light emission time of ~ 2 ns, and mean attenuation length $\lambda_{\rm att}^{\rm sc} \sim 50$ cm. Although α particle releases into ionization an energy of 2.5 MeV, the SC-331 light yield is equivalent to ~ 130 keV. So, signals from neutron are significantly lower than those from relativistic charged particles, and their detection in 200-cm scintillator log is a difficult problem. This problem could be solved by using fiber or strip wave-frequency shifter light-guides with $\lambda_{\rm att}^{\rm shif} \sim 150$ cm.

All the above reactions are characterized by decay of nuclei capturing thermalized neutrons into charged fragments whose energy losses are, in fact, registered. To detect the cascade

neutron yield on the whole, one considers the following additional ways applying the detection of N_γ γ-rays associating the neutron capture and initiating mini-cascades far from the point of neutron capture.

1. The ^{10}B nucleus emits γ-ray with energy $E_\gamma = 0.478$ MeV after the neutron capture.

2. The hydrogen contained in scintillators and polyethylene absorbs neutrons with formation of deuterium nuclei and emits γ-ray with energy $E_\gamma = 2.2$ MeV.

3. The doping of cadmium or gadolinium with a large cross section of absorption of thermalized neutrons ($\sigma_{\rm capt}^{\rm Cd} \sim 5300$ barn, $\sigma_{\rm capt}^{\rm Gd} \sim 60000$ barn) into scintillators (or a covering paint or foil) results in the emission of γ-rays ($\langle N_\gamma \rangle = 4.1 \;\; 4.6$) with the total energy $E_{\gamma\,{\rm tot}} \simeq 16.4$ 13.9 MeV, respectively.

Estimates show that the use of these methods of γ-ray detection makes it possible to increase significantly the efficiency of detection of thermalized neutrons. On the other hand, the disadvantage of such methods is the absence of a correlation between points of neutron generation and detection. So, it would be desirable the use of both the ways of neutron signal detection to improve the performance reliability, to depress the neutron background, and to exclude the appearance of unexpected effects related to unaccounted or unknown processes.

When detecting neutron yield, scintillator detectors operate in the counting mode. The same scintillator detectors must register the ionization component in the amplitude-measurement mode. The signal will be very large in the "knee" energy range. Thus makes it possible to use the difference of amplitudes measured at both the ends of every scintillator log for the determination of coordinates of cascades axes. The accuracy $\delta_x \sim 2$ cm was obtained in test experiments for a scintillator 6-m strip. Besides, NEC-produced signals will be detected by several 2.5-cm width scintillator logs in each layer. If so, the energetically-weighted NEC center is determined in the transverse direction with an accuracy $\delta_y \sim 3$ mm. As the summary accuracy of coordinate measurements for $N_{\rm layer}$ layers is $\delta \sim 1/\sqrt{N_{layer}}$, one can obtain for high-energy cascades the accuracy $\delta \lesssim 1$ mm.

2.3.2 Neutron counters

To detect just neutrons near the points of their generation, one hundred SNM17 200-cm long gas neutron counters (^{3}He, 7 atm) are placed inside the each fifth polyethylene layer at 20 cm intervals (Fig. 10)

2.3.3 Photodetectors

The ionization signal caused by high-energy cascades is assumed to be measured with vacuum phototriodes placed at the opposite ends of scintillator logs. The difference in analogous signals measured by two opposite photodetectors determines the position of the cascade axis. The vacuum phototriodes are characterized by a wide dynamical range ($\simeq 10^7$), simple design, low weight and price, high reliability.

Table 6: Parameters of thermalization and diffusion of 1- and 2-MeV neutrons in pure and borated (0.6%^{10}B) polystyrene, and in a set of 2×2 cm^2-section scintillator detectors made on the basis of polystyrene and coated by 10-μm gadolinium. Code LOENT using BNAB 28-group constants was applied. Neutrons are taken as thermalized at $E_n \leq 0.215$ eV. All values are relative to neutrons avoiding the capture during the thermalization.

Substance	Polystyrene $(CH_2)_n$		Borated polystyrene $(CH_2)_n$+0.6%^{10}B		Polystyrene + 10 μ Gd	
Initial energy of neutron, E_n, MeV	1	2	1	2	1	2
Length of neutron thermalization, L_{therm}, cm	6,38	8,07	3,95	4,97	6,34	8,05
Time of neutron thermalization, τ_{therm}, μs	1.7	1.7	0.83	0.81	1.62	1.63
Length of neutron migration before capture, L_{capt}, cm	10.2	11.5	6.59	8.3	6.66	8.41
Time of neutron diffusion before capture, τ_{capt}, μs	100	99.8	2.45	2.43	4.24	4.23
Loss of neutrons due to capture during thermalization, %	0	0	~ 40	~ 40	0	0

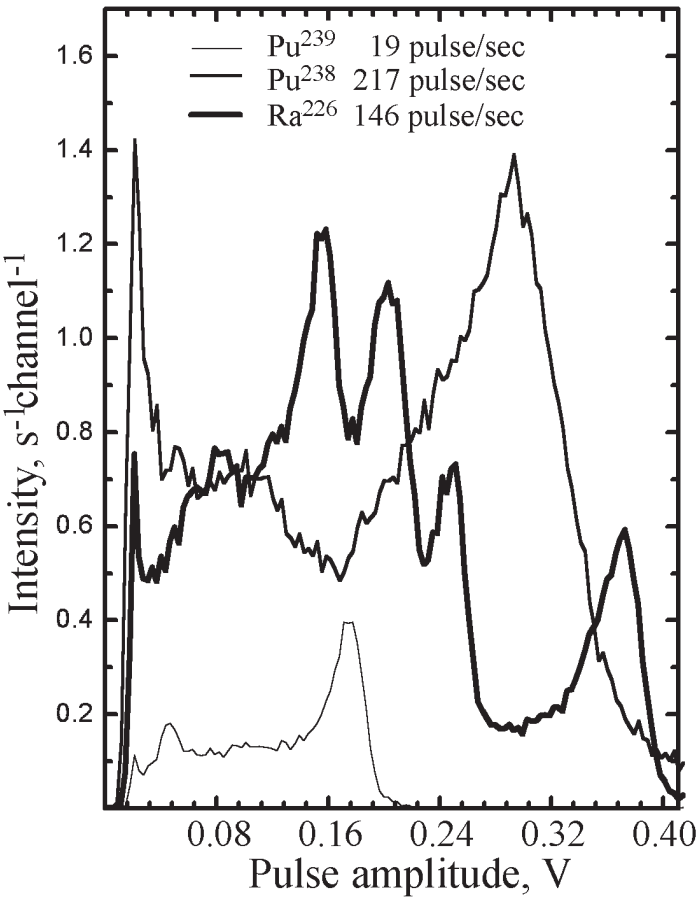

Figure 14: Experimental amplitude spectrum of signals measured by a silicon pixel detector sample.

Neutron-initiated signal in scintillators are to be measured by more sensitive photodetectors. At present we consider the use of PMTs as well as avalanche photodiodes registering signals from optical wavelength shifter fibers passing through scintillators. Besides, the use of newly developed plastic photosensitive plates mounted on surfaces of scintillator logs (several plates per one log) (Fig. 11) that could help to depress the problem of attenuation of low signals.

The detection of delayed γ-rays associating the capture of thermalized neutrons by Cd and Gd nuclei and realizing the higher energy as compared with the neutron capture by ^{10}B nuclei makes it possible to reduce requirements to sensitivity of photodetectors.

2.3.4 Charge detectors

Semiconductor detectors are considered as the main version of charge detectors in the INCA project. However, instead of semiconductor microstrip detectors designed on the basis of *p-i-n* diodes, it is assumed to use silicon pixel detectors elaborated at the present time with our participation. A new concept of local injection mechanism is applied to amplify the drift component of ionization current produced by charged particles passing through the active

bipolar *n-p-n* transistor cell (see details in [1])[1]. A matrix-structure detector consisting of a large number of cells connected into doubled chains is elaborated. The detector are to be characterized with high reliability, sensitivity, signal-to-noise ratio ($\sim 10^2$), linearity, time (~ 1 ns) and lateral ($\sim 10\,\mu$m) resolution. The use of such detectors will make it possible to decrease amplifier requirement and to lighten the suppression of reverse current in the charge detector by the use of temporal and lateral features of the matrix-structure detector.

By now, different versions of detector samples have been manufactured on the basis of silicon with specific resistance ϱ from ~ 20 to ~ 500 Ohm·cm. Fig. 14 shows amplitude spectra of signals measured during the irradiation by α particles emitted by ^{238}Pu, ^{239}Pu, and ^{226}Ra sources of a detector sample consisting of pixels with sensitive regions $l_{\rm pixel} \simeq 75\,\mu$m, placed at $L = 100\,\mu$m intervals and connected in parallel as an open-base circuit. The sensitive area $s_{\rm sens} \sim (l_{\rm pixel}/L)^2$ was $\sim 50\%$ of the total area. One can see in Fig. 14 four peaks corresponding to the detection of α particles from four energy lines of ^{226}Ra source by active pixels and characterized by high output signal amplitudes achieved without external amplification. The muse of silicon with a higher specific resistance $\varrho \gtrsim 500$ Ohm·cm will make it possible to increase the dimension of sensitive pixels. The transfer to smaller technological base dimensions ($l_{\rm base} \sim 1\ \mu$) will make it possible to increase the amplification factor of single-pixel signal being proportional to $\sim (l_{\rm pixel}/l_{\rm base})^2$. The use of all the above-mentioned factors are to make it possible to fill the detector area by sensitive pixels $s_{\rm sens} \sim 100\%$. At present it is assumed to join cells into 5.5×5.5 cm^2 sections. Along with the above-stated approach, more traditional way of looking the charge detector is possible as well.

[1]Detectors are under elaboration. Companies interested could participate in this work and get information at sites of the International Science and Technology Center (ISTC) (http://www.istc.ru/istc/website.nsf/fm/ISTC+Ru, by using links: (1) "tech-db.istc.ru"; (2) "ISTC Projects"; (3) "By Number" (in "All Projects"), search for project # 3024) and Foundation for Assistance to Small Innovative Enterprises (FASIE) (http://www.fasie.ru/eng/)

2.4 Data acquisition system of the INCA

The planned INCA's data acquisition system (DAQ) must fulfil the following functions:

1. Elaboration of a trigger system in the moment of nuclear-electromagnetic cascades development inside the calorimeter.
2. Collection amplitude analysis and saving of data concerning electron-photon component.
3. Registering the pulses from neutron detectors and saving their count.
4. Search for the direct neutrons from solar flares.

Block diagram of the DAQ is shown in 2.4. Like all other constituents of the considered project, this scheme is modifying constantly, in accordance with permanent development of the microelectronics' elemental base and appearing of the new types of electronic components.

2.4.1 Trigger scheme

In the INCA project, the photo-triodes, avalanche diodes and compact photomultipliers are used for scintillation bursts conversion into electrical signals.

The pulses from photo-triodes, which are mounted at the edges of scintillator logs, are coming to the trigger elaboration scheme. Inside, analogous signals from scintillators of every detector plane are united; the scheme's output voltage at any time being proportional to the total number and sum amplitude of the simultaneous scintillation signals from considered plane. Should the sum voltage of some plane exceed a predefined threshold value at some time moment, the scheme would generate a control signal - trigger, which causes the control processor to start the data registration program in calorimeter.

Summing of the analogue pulses from same-plane detectors is supposed to fulfill by a classic resistor or capacity voltage divider with operational amplifier K144UD2 (CA3130), comparison of the sum signals with the threshold - by a K597CA3 (AM685) type integral comparator.

To enhance the reliability of cascade selection and to reduce the intensity of background events, more strictly trigger conditions may be applied. Hence, one could demand, that the trigger should be elaborated only in the case of simultaneous threshold exceeding in neighboring detector planes, one should provide the possibility to change the trigger threshold during the measurements immediately by the commands of control processor and so on. It is obvious, that such tasks are easily solved by the means of the modern CMOS logic chips with reduced power consumption.

2.4.2 Amplitude analysis

Trigger signal elaborated by a summing scheme starts the amplitude-digital converters (ADC) present in each registration channel. ADCs assure the transfer of the photo-detector pulse amplitudes into digital codes.

We intend to base the INCA's converters on the integral ADC chips of AD7887 types. The chips possess a high operation speed (8 mcs per conversion cycle) and low power consumption (3.5 mW in normal operation mode with the possibility to reduce down to 5 mcW in

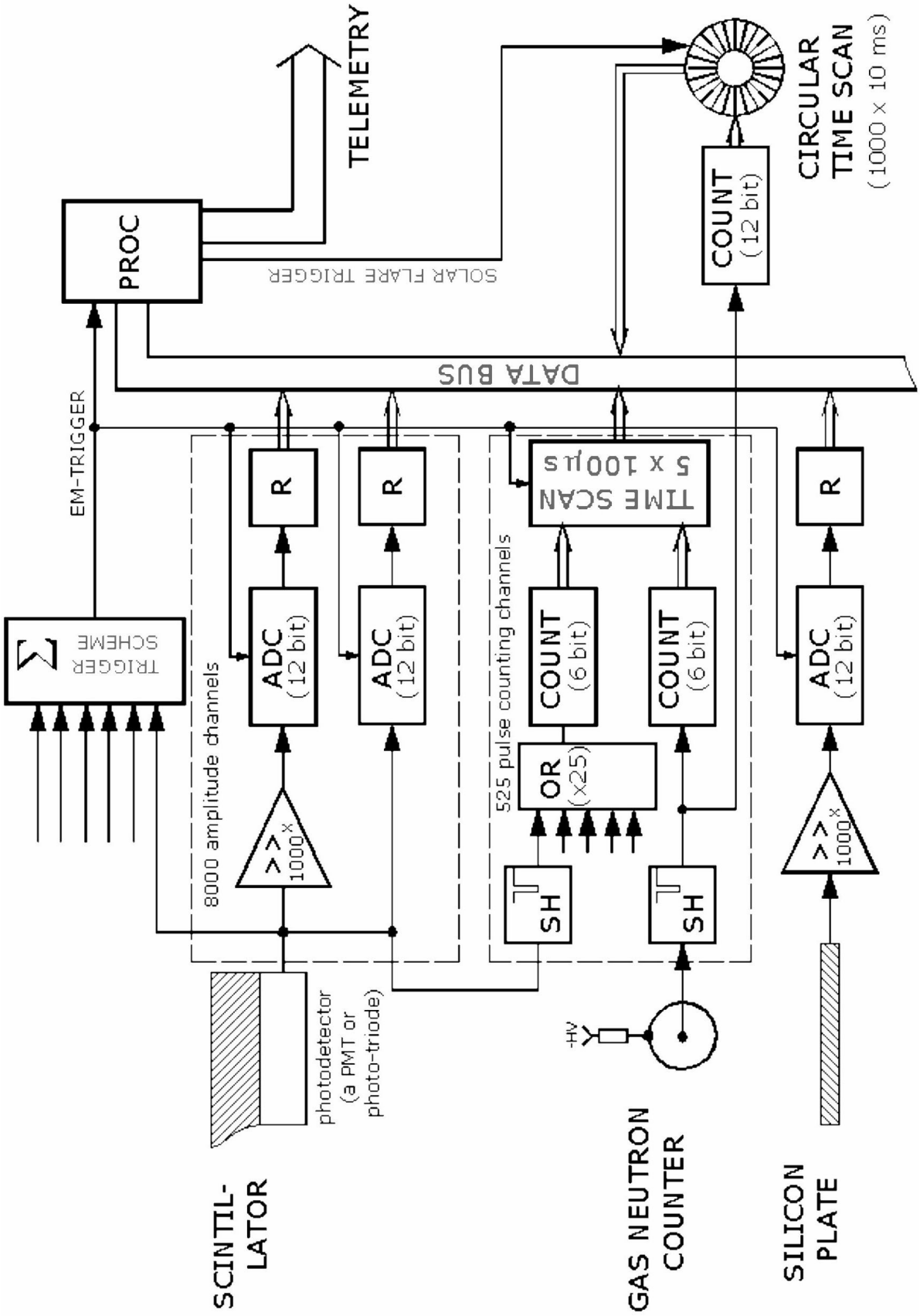

Figure 15: Data acquisition system of the INCA.

standby mode). Each chip having a dynamical range about 4000 (2^{12}) and the awaiting range of scintillation amplitudes being of the order of $10^5 - 10^6$, there must be two ADC elements in every channel with different sensitivities. The low-sensitive ADC chip must obtain its input signals from a photo-detector immediately, whilst the high-sensitive one – through a $1000^{\times}$ linear amplifier build on the K144UD2 chip. Hence, whatever the input signal amplitude would be, one of ADC chips occurs in its linear diapason, their common dynamical range being about $1.6 \cdot 10^6$ (2^{24}).

The AD7887 chip's output amplitude code being given sequentially, it must be converted into parallel bytes before to be loaded into processor memory. This operation is fulfilled by shifting registers on the CMOS chips of the 564IR13 (MM54C905) type. Such CMOS chip containing a 12-bit register, two chips of the said type are necessary in each channel (with 24 data lines in common bus). Otherwise, one could use only register chip per a channel and a 12-line data bus, with stepwise data reading from the internal ADCs memory. The corresponding dead time increase and the necessity of a more complicated logic for data selection control are drawbacks of second approach.

Output pins of the shit registers are connected immediately to the lines of the system's common information exchange bus. Selection of a certain registration channel is fulfilled according to the address code set by the control processor. Address code is analysed by decoder chips of the type K1533ID3(74LS154). The total number of amplitude channels being 8000 and each K1533ID3 chip having only 16 output pins, data reading system must be organised hierarchically, amount of decoder chips being about 4100 (16^3) and the number of address lines in common system bus being 16.

Amplitude channels destined for operation with the signals of avalanche diodes (about 500) are build according to the same principle. Characteristic feature of these photo-detectors is their exclusively high quantum efficiency making it possible to measure the signals from the single relativistic particles.

2.4.3 Counting of neutron pulses

Energy of the hadron component of a nuclear-electromagnetic cascade developing in INCA can be estimated according to the number of pulses from neutron detectors arrived in duration of the "time gate" – a fixed time interval after the trigger signal. Since there are the thermal neutrons that are detected in process of their diffusion, registration of neutron pulses could proceed by the same scintillation detectors as that of electron-photon component. Two conditions must be satisfied for the purpose: the beginning of neutron signal's sampling would be late for $5-10$mcs relative to trigger and the total length of time gate would be about $\sim 2.5-3\ \tau_{\rm capt}$, i.e., $300-500$ mcs in the case of INCA. The short preliminary delay is necessary both to exclude fully the electromagnetic signals from the count and to give a time for evaporation neutrons born in developing cascade to lose their energies down to thermal values.

The considered INCA project provides two methods for neutron registration. The first is the staining of outer sides of scintillation logs with Ca- or Gd-containing paints, the other one

– placement of the gas proportional counters inside the calorimeter. In the first case, intensive captures of the thermal neutrons by Ca or Gd nuclei result in emission of -rays being registered by scintillator. In the second one, the ^{10} isotope enriched BF_3 or ^{3}He gases must be present in counters filling; neutron registration proceeds thanks to charged products of the reactions ^{10}B(n,α)^{7}Li or ^{3}He(n,p)^{3}H, respectively.

The block diagram shown in Fig. 2.4, takes into account both methods of neutron registration. Hence, the signals from photo-triodes, parallel to ADC, are connected to shapers, which generate digital pulses having standard amplitude and duration. Digital pulses are united by logical "OR" elements for every group of 25 neighbouring scintillators and are counted afterwards during the after-trigger time gate by a binary counter. The same "shaper-counter" pairs are used also in the channels operating together with neutron counters.

Pulse shapers used in counting channels, consist of an amplifier having a gain about $\sim 30-60$ and a standard univibrator. Amplifiers could be build on the integral 514UD2 type chips or low-powered transistors. As univibrator the 561AG1 ((CD4098BE) type chips may be used. Counting of digital pulses may be fulfilled by the 176IE1 or 176IE2(TA5971) chips having 64 (2^6) or 32 (2^5) capacity, respectively.

The binary codes of neutron pulse numbers are stored in the counters in a set $(5-10)$ of consecutive time intervals, 100 mcs in duration each. After the end of each interval, these codes are written in a peripheral memory block, separately for every registration channel. As a result, this peripheral memory, called the "time scan" block, accumulates the data about time behaviour of neutron intensity during the time gate period. Depending on the number of time intervals, the total capacity of time scan memory must be about $40-80$ kB.

Zero point of time counting in each neutron event coincides with the moment of trigger signal.

Management of the time scan system (reckoning of the 100 mcs intervals, formation of the address codes and control signals for peripheral memory) is fulfilled by a separate controller which is autonomous relative to the central processor. After the $500-1000$ mcs after the trigger this controller signals to processor its readiness for output of time scan data.

2.4.4 Search for the direct solar flare neutrons.

It is supposed, that characteristic feature of the events, connected with the neutrons coming immediately from the Sun in the moments of flares on its surface, is their relatively long duration. Hence, the awaiting length of the time, when neutron intensity exceeds the background, is about tens and hundreds of milliseconds. To search such events, a special large-capacity time scan system is foreseen in the INCA's DAQ system. This time scan memory provides the memory for keeping 1000 counts for each of 100 gas neutron counters. Standardized digital pulses from the counters are connected to the inputs of this system.

Unlike the short time scans of the INCA's count channels, which are described above, the data in the considered system are written continuously in a ring-like manner: when the memory address counter achieves the last memory cell, it resets to zero, starting another cycle of

memory filling. A long duration of time intervals (about 10 ms) being accepted in this system, the ring memory constantly keeps information about the behaviour of neutron intensity during the period of the last 10 s . (Of course, pulse counters of higher capacity than that of count channels must be used here; they could be build on the cascaded elements of the same 176IE1 or 176IE2 type).

Scanning of neutron intensity in the ring system ceases after the signal of a solar flare. As such, one could use a signal from international solar flares service or elaborate a separate trigger from the Sun-oriented crystal NaI scintillators which register the γ- and X-ray emission of a flare. After the control signal coming, the scan continues during a half of a total number of time intervals (i.e. about 5 s), stops then and its controller says to central processor about the readiness for data output.

2.4.5 The hard- and software demands

Operation of the INCA's DAQ system is supposed to functionate under the control of specialized registration programs and one of the modern real-time operational systems, QNX for example.

The total size of the "raw" information coming from INCA's detectors in registration of a single event is ~ 1 Mb. As shows the experience of exploitation of analogous DAQ systems at Tien Shan mountain station, fetching of such information volume takes a time about $0.3 - 0.5$ s (using the standard PCI type buses and ~ 1 GHz tact frequency processors). Duration of the same order will have the INCA's dead time after registration of each particular event. Data archiving with the use of standard compression mechanisms results in a $80 - 90\%$ volume reducing. Hence, the modern hard disks, 100-200 Gb in capacity, permit to store about $0.5 - 1$ million of registered events.

All the DAQ system elements considered above (the summing trigger scheme, 12-bit amplitude analyzers, pulse shapers and pulse counters, various kinds of time scan modules) at present time are realized on the integral TTL-elements and are widely used in extensive air showers experiments at Tien-Shan mountain station so as in test measurements at the Serpukhov U-70 accelerator. In particular, the DAQ system of the big ionization-neutron calorimeter INCA-44 being created now at Tien-Shan as a part of the complex "ATHLET" program, corresponds to the block diagram of Fig. 2.4. For the use of the same electronics in the space INCA experiment, no logical changes but only modernization with the use on modern element base (such as CMOS and CPLD chips) are needed.

3 Conceptual fundamentals of the INCA project

One of the most important fundamental concepts of the INCA project is the use of alternate layers of substances with a minimum and maximum atomic-mass weights. It is related, on the one hand, to a fact that the cross section of hadron interaction with light materials rises much faster as compared with heavy substances (by $\sim 10\%$ at increasing energy by one order in magnitude). On the second hand, heavy substances are applied to generate neutrons whose yield increases nonlinearly with atomic number and is of the type of $\sim A^2$ (i.e. it increases by a factor of two when passing from lead to uranium). Given a fixed instrument weight, the absorber's maximum thickness (in terms of mean free path for interaction) and the maximum neutron yield used for energy measurement and electron separation are achieved.

Analysis of experimental data derived, on the one hand, with the use of so complicated instrument, uncontemplated device response fluctuating even at given parameters of particles detected by the instrument, and, on the second hand, characterized by such uncontrolled natural factors as energies, types, arrival directions and places of particles, points of their interactions is impossible without a detailed simulation of processes occurring in the instrument, especially in the case of the use of new ideas and concepts. To present day, estimation simulations have been carried out being necessary (a) to elaborate the concept of the ionization-neutron calorimeter; (b) to estimate the accuracy of the measurement of cascade energy initiated by protons and nuclei in the energy range $10^{15} - 10^{16}$ eV by detecting the ionization and neutron signals; (c) to estimate quantitatively a possibility to reject proton-initiated showers, i.e., efficiency of separation of electron-initiated cascades against the background of cascades caused by primary protons and nuclei. The modified MC0 code [53] was used, which takes into account (a) quark-gluon string model of hadron interactions [54]; (b) a lot of accelerator data including generation of jets, resonances, charm particles. In doing so, (1) energy loss for ionization and Compton effect, generation of evaporated neutrons by excited nuclei after (i) hadron interactions, (ii) inelastic interactions of γ-rays, (iii) low-energy γ-ray absorption vie giant resonance process were taken into account.

To understand well effects caused by the layered structure, we have simulated processes in a setup with a periodic structure, so that each layer contained lead or a light substance (polyethylene, e.g.) with a thickness of 10 and 20 g/cm^2, respectively. As far as evaporated neutrons are concerned only the process of their generation was considered but not the further behavior. A more detailed analysis of the neutron thermalization and diffusion in the setup with allowance for edge effects and the efficiency of both neutron and charge-particle counters will be carried out in the nearest future with the use of modern codes (GEANT, SHIELD [55, 56]) as well. We will investigate the role of the primary spectrum, real INCA's geometry, apparatus response and so on. However, we believe that the results given in the present paper will not be subjected to a qualitative change.

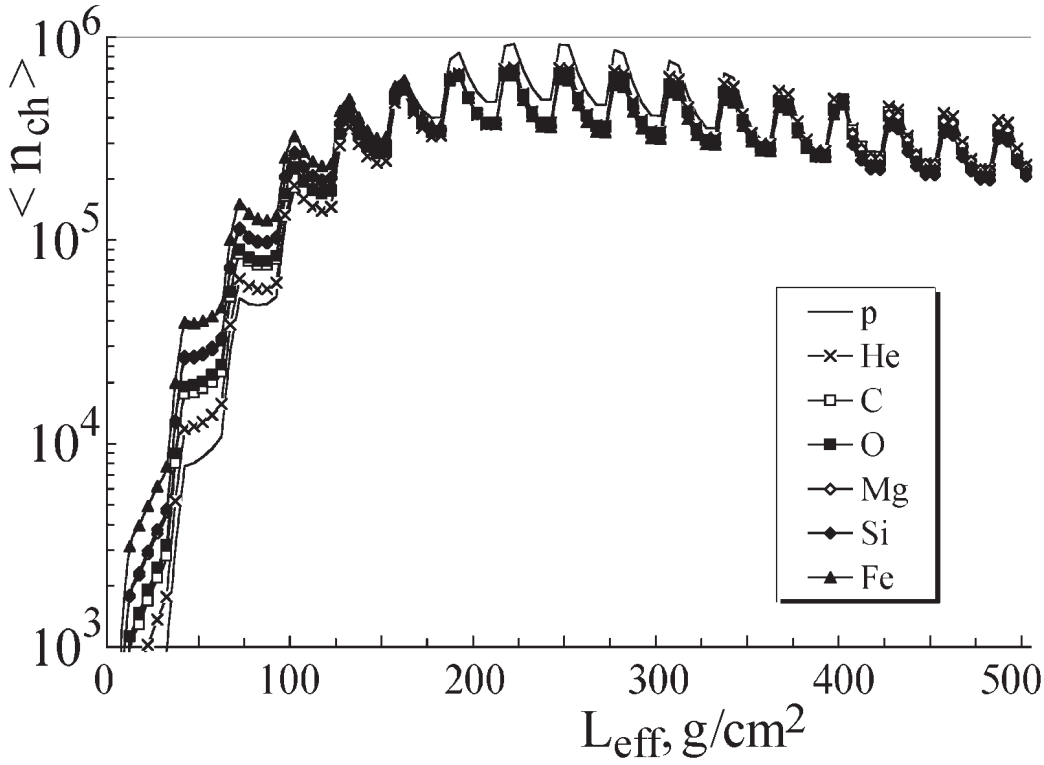

Figure 16: L_{eff} dependence of number of charged particles in cascades initiated by 1-PeV protons and nuclei.

3.1 Measurement of primary particle energy

Energy measurement by ionization signal

Potentialities of the INCA in measuring energies of various PCR nuclei are illustrated in Fig. 16, which displays dependences on L_{eff}– effective NEC length for secondary charged particles in cascades initiated by 1-PeV protons and nuclei. The peculiar kind of distributions with numerous peaks is explained by the INCA's multilayer structure including both heavy and light materials.

As is seen, the maximum number of secondary charged particles corresponds to an absorber depth of $200 - 300$ g·cm^{-2}. Beginning from this depth, cascade curves are, in fact, independent of mass of projectile nuclei. At smaller depths, the signal highly depends on primary particle type (see Sect. 3.3). At lower energies, the cascade maximum is shifted towards the NEC origin point.

The accuracy of energy measurement depends, first of all, on dispersion of the number of cascade charged particles, $\sigma^2(n_{ch})$. Fig. 17 demonstrates L_{eff} dependence of the $\sigma(n_{ch})/\langle n_{ch}\rangle$ ratio for a number of secondary charged particles found by integrating over L_{eff}, in cascades initiated by primary protons and nuclei with energies () 10 TeV and (b) 1 PeV. As is seen in Fig. 17, the relative accuracy of measurement is poor at the initial cascade stage and achieves a good-enough value ($\sim 30\%$ for protons and 10% to 20% for nuclei) at the cascade-maximum depth ($250 - 300$ g·cm^{-2}. The use of the initial stage just decreases the energy measurement

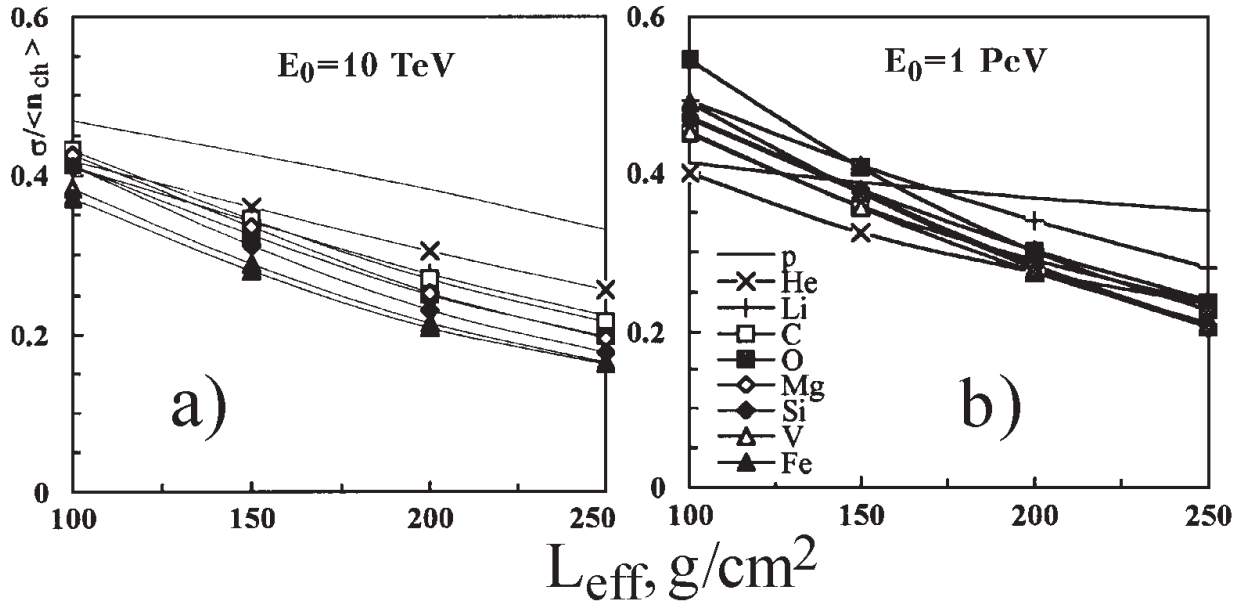

Figure 17: $L_{\rm eff}$ dependence of the $\sigma(n_{ch})/\langle n_{ch}\rangle$ ratio for number of charged particles in cascades initiated by protons and nuclei with energies () 10 TeV and (b) 1 PeV.

accuracy being optimal near the NEC maximum.

Energy measurement by neutron signal

It is very important that the total amplitude of the evaporation neutron signal can also serve as an additional and independent information on the primary particle energy. It has been taken in simulation that the average multiplicity of evaporated neutrons, $\langle n'_n\rangle$, generated per one simulated inelastic hadron-nucleus (or photon-nucleus) interaction with lead nucleus varies interaction energy from ~ 1 at 10 MeV to ~ 25 at 2 GeV and is almost constant at $E \gtrsim 10$ GeV ($\langle n'_n\rangle \approx 26$). As is seen, the energy dependence is very weak at $E \gtrsim 2$ GeV. This makes it possible to use the neutron signal for energy measurements at sufficiently high energies ($E \gg 10$ GeV) of primary particles. Hadron interactions provide the predominant contribution ($\gtrsim 60\%$) into the neutron yield even at the initial stage ($x \lesssim 100$ g·cm^{-2}) of proton-initiated NEC development at energies under consideration. This contribution increases with energy, while the corresponding fraction in electron-initiated cascades is equal to $\sim 5\%$ (in this case $\sim 95\%$ of neutrons are generated through the giant resonance and inelastic interactions of γ-rays).

As is seen from Fig. 18, the energy dependence of the total neutron number integrated over various values of effective NEC length $L_{\rm eff}$ in cascades initiated by protons is monotonous and, in fact, almost linear (in the doubly logarithmic scale). Dependences for primary nuclei demonstrate the similar behavior.

As is seen from Fig. 19, the magnitude difference of evaporation-neutron yields in proton- and iron-initiated cascades does not exceed the factor of two beginning from ~ 200 g·cm^{-2}. At small depths the signal highly correlates with primary particle type (see Sect. 3.3).

Fig. 20, wherein the $L_{\rm eff}$ dependence of the $\sigma(n_{neut})/\langle n_{neut}\rangle$ ratio for the evaporation

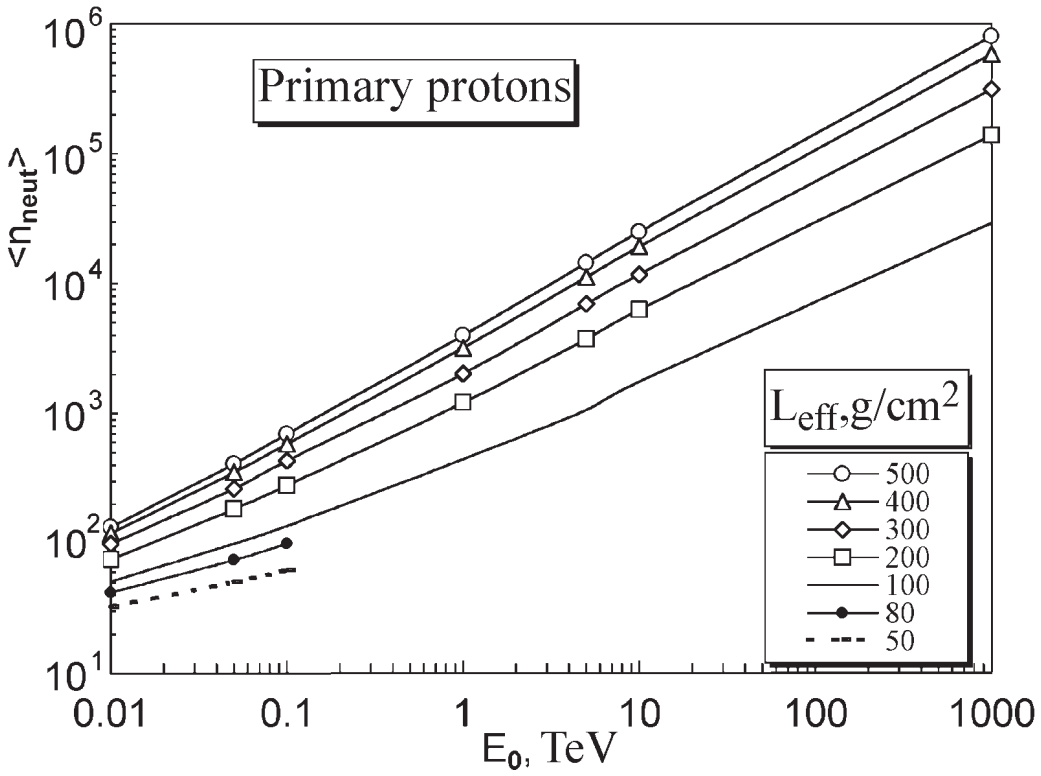

Figure 18: Energy dependence of the total number of the total average evaporated neutron number at $L_{\text{eff}} = 500, 400, 300, 200, 100, 80, 50$ g/cm^2.

neutron component is shown, demonstrates the accuracy of energy measurement by neutron signal. Here n_{neut} is the number of neutrons found by the integration over L_{eff} in cascades initiated by 1-PeV protons and nuclei.

As is seen in Fig. 20, the relative accuracy of measurement is shown, the corresponding standard deviation of energy distribution can also be about $(20 - 30)\%$ for various nuclei.

the relative accuracy of measurement is poor at the initial cascade stage and achieves a good-enough value ($\sim 30\%$ for protons and 10% to 20% for nuclei) at the cascade-maximum depth (~ 300 g·cm^{-2}. The use of the initial stage decreases the energy measurement accuracy being optimal near the NEC maximum as well as in the case of the use of ionization component.

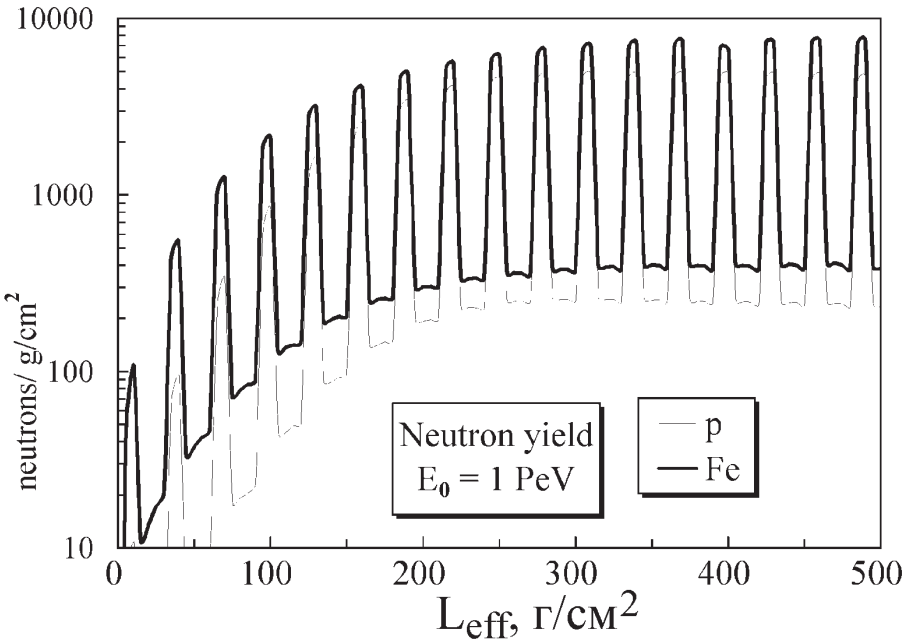

Figure 19: L_{eff} dependence of the average evaporated neutron yield (per 1 g/cm^2) in cascades initiated by 1-PeV protons and iron nuclei.

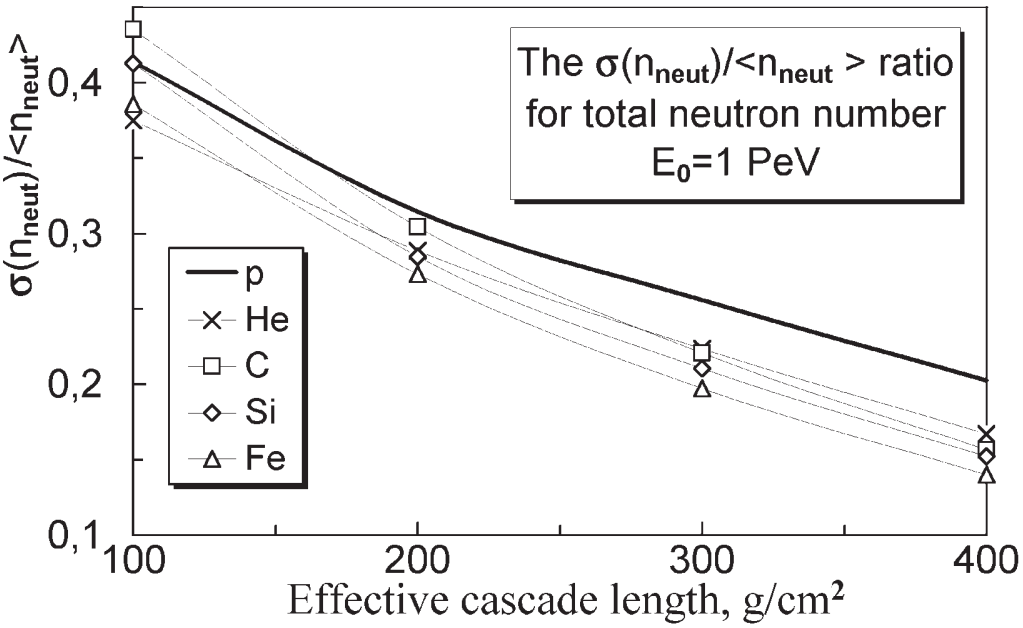

Figure 20: L_{eff} dependence of the $\sigma(N_{neut})/\langle N_{neut}\rangle$ ratio in cascades initiated by 1-PeV protons and nuclei.

3.2 Separation of primary electrons against proton background

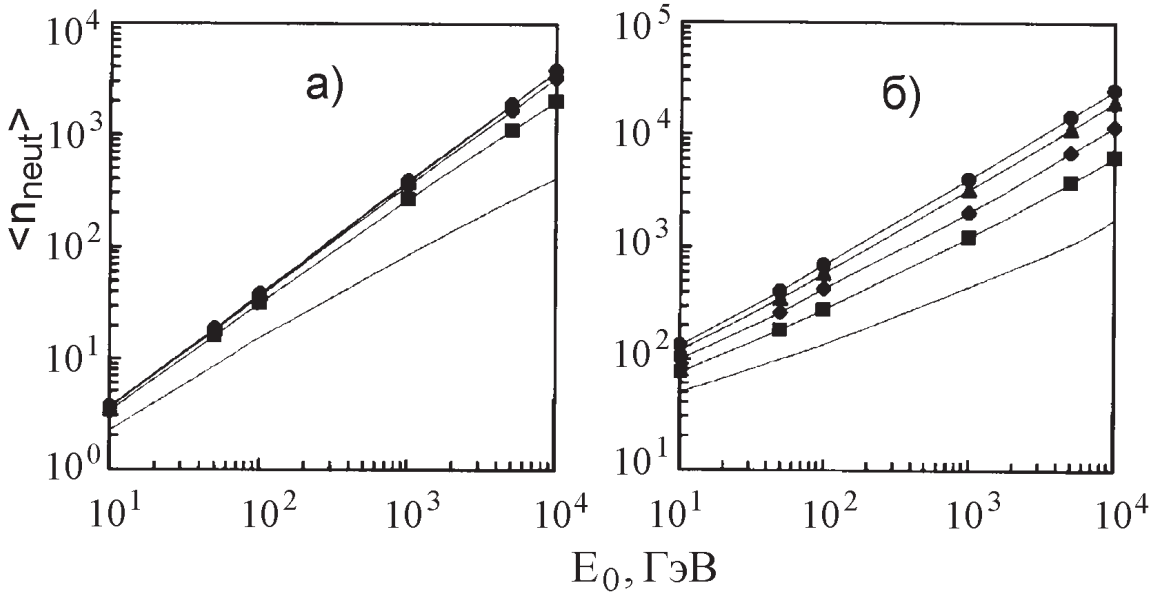

Figure 21: Energy dependence of the total number of evaporated neutrons, $\langle n_{neut} \rangle$, in NECs initiated by (a) electrons and (b) protons for different L_{eff}: black circles, triangles, rhombuses, squares, and line correspond to $L_{\text{eff}} = 500$, 400, 300, 200, 100 g·cm^{-2}.

The proton flux exceeds the electron flux by about three orders of magnitude. However, there exist certain possibilities to separate electrons against the predominant proton-produced background. Generally, two procedures are applied to suppress (reject) the background characterized by factors K_1 and K_2.

(1) When fixing the cascade starting point within the first lead-absorber layer with a thickness of $\Delta x \sim 10$ g·cm^{-2}, then the fraction of protons is $K_1 = \Delta x / \lambda_{int}^{p-Pb} \simeq 1/20$, i.e., $\sim (1 - K_1) \simeq 95\%$ of proton-initiated cascades are discriminated.

(2) When protons release in the first interaction into the electromagnetic component the energy E_γ, its average energy is $\langle E_p \rangle \approx E_\gamma / K_\gamma \approx 5E_\gamma$. Since the integral proton spectrum decreases as ${}_p(> E_p) \propto E_p^{-1.7}$, the ratio of the effective flux of protons producing the same energy release, E_γ, as electrons with an energy E_e, to $I_p(> E_p)$ is determined by the factor $K_2 \simeq 0.2^{1.7} \simeq 1/15$. I.e., $\sim (1 - K_2) \simeq 93\%$ of proton-initiated cascades are discriminated.

The use of K_1 and K_2 factors keeps a small ($K_1 \times K_2 \simeq 3 \times 10^{-3}$) fraction of proton-initiated cascades which could imitate electron-initiated cascades. The detection of evaporated neutrons makes it possible to apply a a new powerful rejection factor.

An energy dependence of the average number of evaporated neutrons $\langle n_{neut} \rangle$ in electron- and proton-initiated cascades as a function of L_{eff} is shown in Fig. 21. One can see a significant distinction between cascades of different nature. However, it is obvious that an effective separation is only possible in the case of an effective disjunction of the corresponding distributions. Simulations show that at a sufficient value of $L_{\text{eff}} \gtrsim 100$ g·cm^{-2} the overlapping of distributions of number of evaporated neutrons in electron- and proton-initiated cascades is rather small.

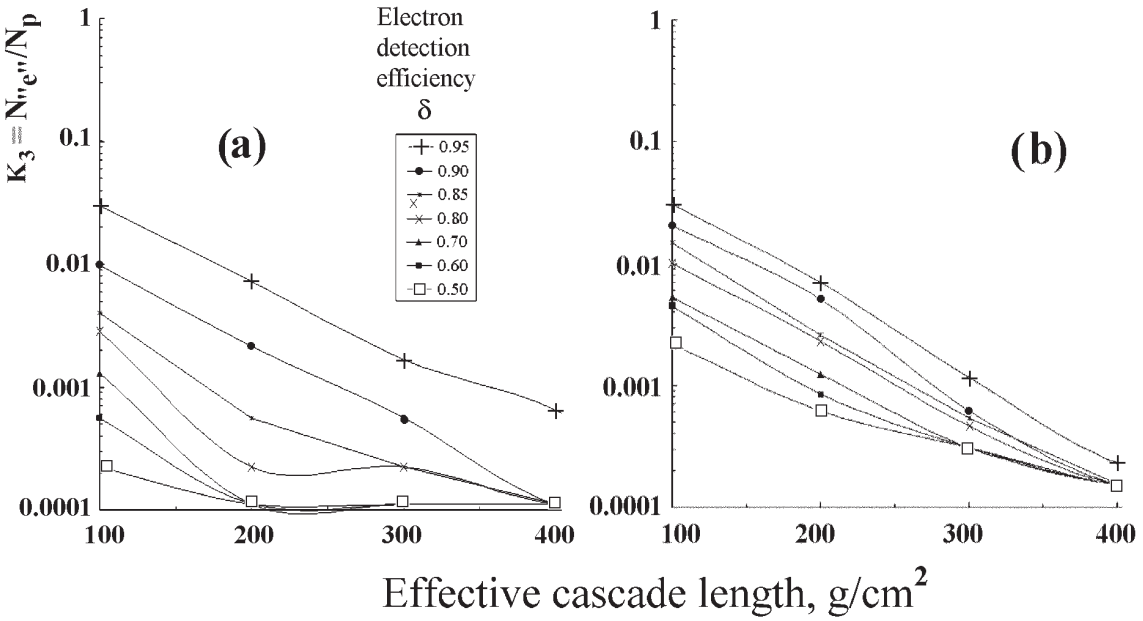

Figure 22: Rejection factor K_3 for electron-like proton-initiated cascades as a function of effective cascade length L_{eff} for various prescribed electron detection efficiency δ at (a) $E_e = 100$ GeV and (b) $E_e = 1000$ GeV.

The INCA concept uses this property as a new criterion for rejection of electron-like proton-initiated cascades in addition to the first and second criteria. Quantitatively, this idea can be described by the rejection factor (K_3) which depends on both the absorber thickness and prescribed efficiency δ of the primary electron/γ-ray detection (Fig. 22). Here δ is the fraction of electron-initiated cascades, which remain after the rejection of electron-initiated cascades from the range of overlapping distributions. Even for a thin (~ 100 g·cm^{-2}) instrument, $K_3 \approx 10^{-2}$ at δ =0.9. Simulations show that the K_3 factor depends on E_e rather weakly up to 10 TeV. Besides, we can realize the K_3 criterion even if the neutron detection efficiency is as low as $10 - 20\%$.

When applying the detection of evaporated neutrons to separate electron-initiated cascades, it is very important to take into account the neutron background caused by low-energy particles. Its intensity could be estimated as follows. The number of neutrons generated in the total volume of the INCA instrument in the time t_{meas} is equal to $N_{\text{neutr}} \simeq J_{\text{CR}}(> E_{\min}) \Gamma^* t_{\text{meas}} \langle n_{\text{neutr}}(n(E_0, L_{\text{eff}}))\rangle$, where $J_{\text{CR}}(> E_{\min})$ is the integral intensity of PCR particles with energies $E > E_{\min}$; $\Gamma^* = C_{\text{E}} \cdot \Gamma'_{\max} = 3.2 \cdot 10^5$ cm^{2}sr is the INCA's maximum geometric factor; $t_{\text{meas}} = 3 \cdot 10^{-4}$ s is the time of neutron counting in the events under consideration; $\langle n_{\text{neutr}}(n(E_0, L_{\text{eff}}))\rangle$ is the average number of neutrons generated in the volume by cascades with the effective length L_{eff} produced by PCR particles with energy E_0. In accordance with [57] in high and low latitudes, respectively, $J_{\text{CR}}(> E_{\min}) = 0.3$ 0.015 cm^{-2-1}sr^{-1}, $E_{\min} = 2$ and 15 GeV, and $N_{\text{CR}} = 45$ 2.3. For the isotropic irradiation of a cube with the side L, the average geometric path passed by particles from the entry in to the exit from the cube is $\langle l \rangle = \frac{2}{3}L$, that corresponds to the matter quantity $\langle l\varrho \rangle = \frac{2}{3}L\varrho = 166$ g·cm^{-2}.

As the mean free path (m.f.p.) for the first interaction of a primary proton is $\lambda_{\rm int} \approx 85$ g·cm^{-2} (at $E_p \simeq n$ GeV), the effective length of the mean cascade is $L_{\rm eff} = l\varrho - \lambda_{\rm int} \approx 80$ g·cm^{-2}. Then we substitute the calculated dependence $n(E_0, L_{\rm eff})$ (Fig. 18) into the expression for $\langle n_{\rm neutr}(n(E_0, L_{\rm eff}))\rangle$, and using it we get that the average total number of neutrons generated inside the instrument in the time $t_{\rm meas} = 3 \cdot 10^{-4}$ s is equal to $N_{\rm neutr} \sim 965 \pm 145$ 100 ± 65 in high and low latitudes, respectively, that is significantly lower than the number of neutrons in proton-initiated NECs in the interesting energy range $10^{12} - 10^{16}$ eV.

If we could select the region wherein cascade neutrons are generated, thermalized, and captured, than the background will be proportional to its volume. As the paths for neutron thermalization and capture in the borated polyethylene are equal to $L_{\rm therm} \lesssim 6$ cm and $L_{\rm capt} \lesssim 10$ cm, then the transverse linear dimension of the effective region being of our interest could be estimated to be as large as $L_{\rm tr} \simeq 20$ cm. Thus, the effective volume is $\sim 1\%$ of the total volume even for cascades originated at the border and passing through the whole instrument ($200 \times 200 \times 200$ cm^3) (this value could be rather larger due to an insufficiently efficient allocation of the generation region). The background intensity decreases equally. Furthermore, simulations show (Table 6) that the doping of ^{10}B, Cd or Gd into the scintillator, first of all, decreases both $L_{\rm therm}$ and$L_{\rm capt}$, i.e., decreases the effective region, and, secondly, decreases significantly the time of neutron capture, $\tau_{\rm capt}$, that makes it possible to decrease the time of neutron counting, $t_{\rm meas}$. Finally, all these factors make it possible to decrease very essentially the background intensity.

3.3 Estimation of mass number. Search for "Centauros"

Both the neutron and ionization signals could be used to estimate the mass number of primary particles at the cascade initial stage. As Figs. 23 and 24 demonstrate, the difference in amplitude between cascades initiated by protons and iron nuclei could be as large as one order of magnitude. This is valid for both the neutron and ionization signals.

Figs. 25 and 26 show distributions of charged particle multiplicity at a depth of 50 g·cm^{-2} and total neutron number found by integrating over the effective thickness $\Delta = 40$ g·cm^{-2}, respectively, for cascades initiated by primary protons and nuclei with the energy $E_0 = 1$ PeV. As is seen, distributions for different kinds of particles are essentially distinctive, although some overlapping takes place.

Simulations show that standard deviations of differential neutron-number distributions in relatively thin layers are equal to $\sim 35\%$ and $\sim 15\%$ for cascades initiated by primary protons and nuclei, respectively. This makes it possible to separate the main nuclear groups (p, He, CNO, ..., Fe).

At the same time it is possible to detect hypothetical particles with very high masses and relatively low charge. However, it requires the detection of neutrons generated just at the initial cascade stage but not the total neutron number.

At least, just this method of attack is related to the problem of search for hypothetical "Centauros", i.e., hadron interactions seeming as the generation of stable hadrons (baryons,

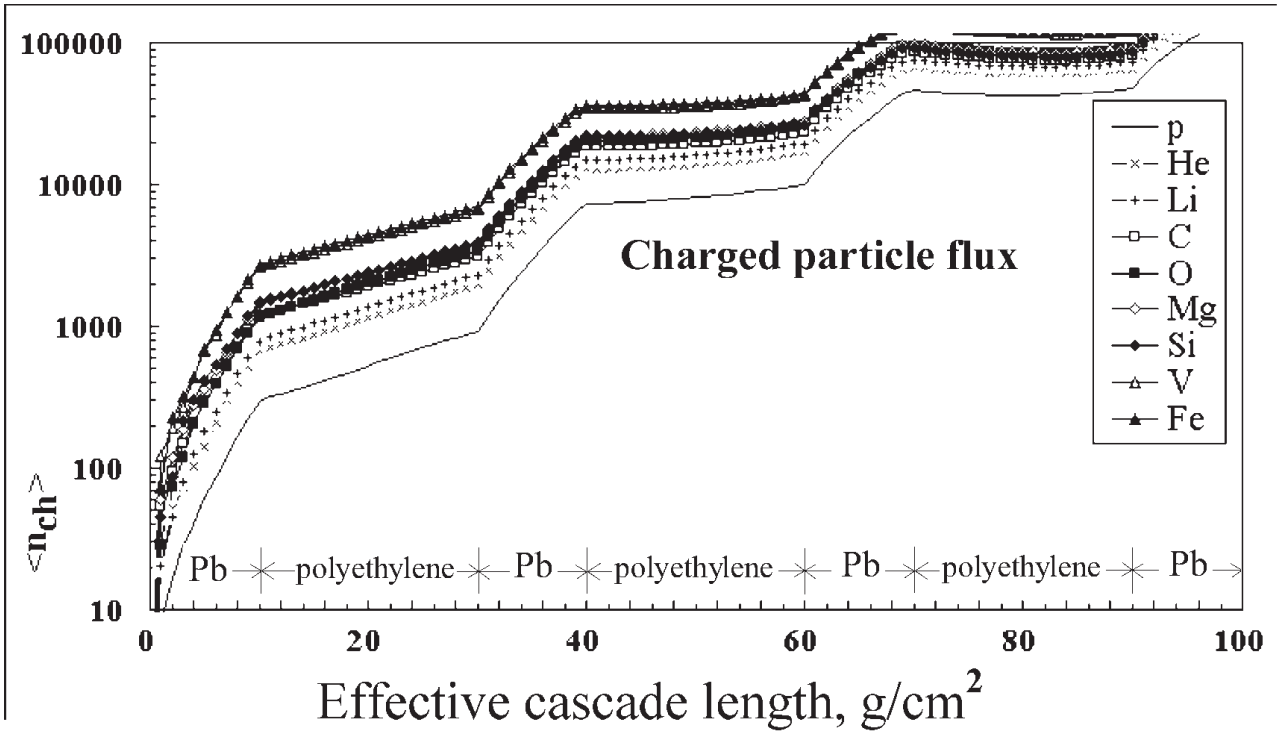

Figure 23: L_{eff} dependence of the charged particle multiplicity at the cascade initial stage for primary protons and nuclei at $E_0 = 1$ PeV.

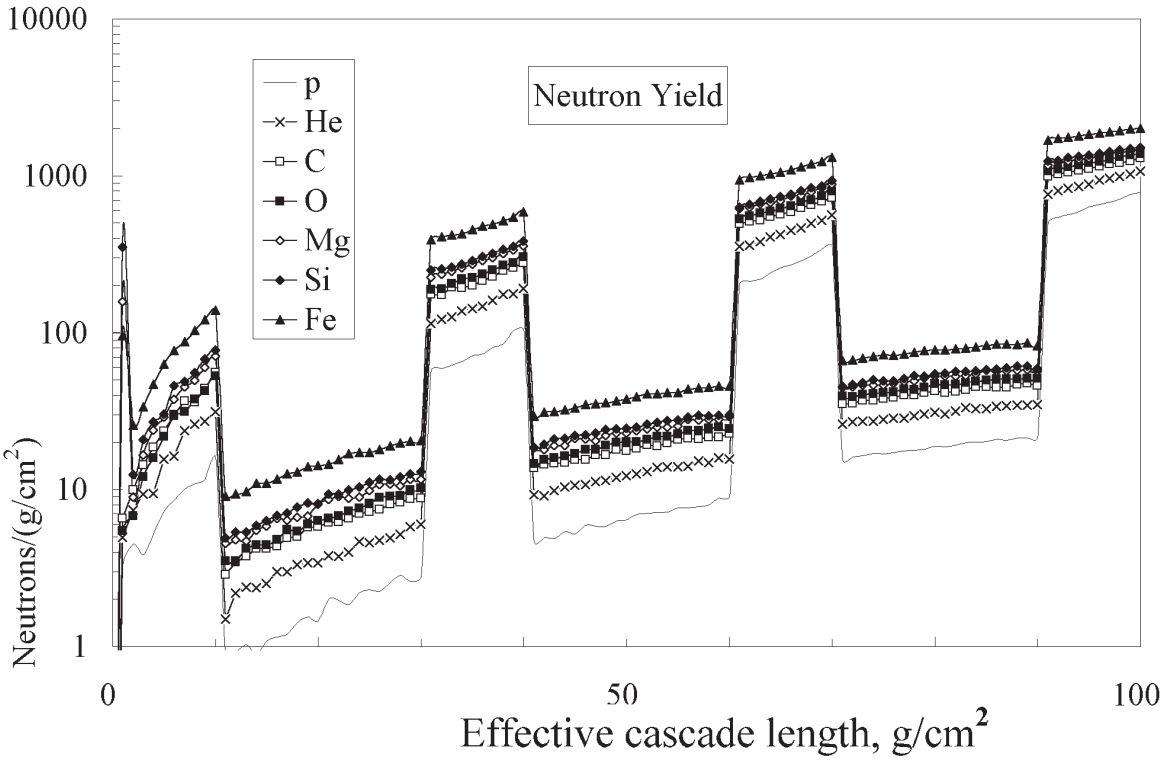

Figure 24: L_{eff} dependence of the average intensity of evaporated neutron generation (per 1 g·cm^{-2}) at the cascade initial stage for primary protons and nuclei at $E_0 = 1$ PeV.

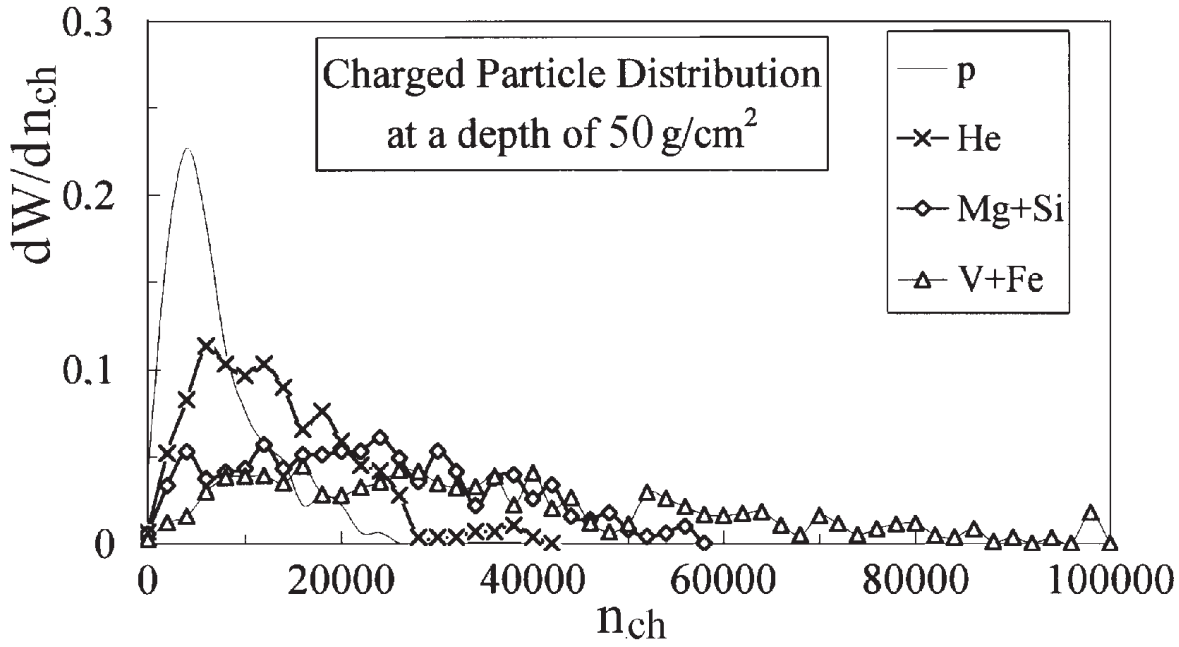

Figure 25: Distribution of charged particle multiplicity at a depth of 50 g·cm^{-2} for cascades initiated by primary protons and nuclei at $E_0 = 1$ PeV.

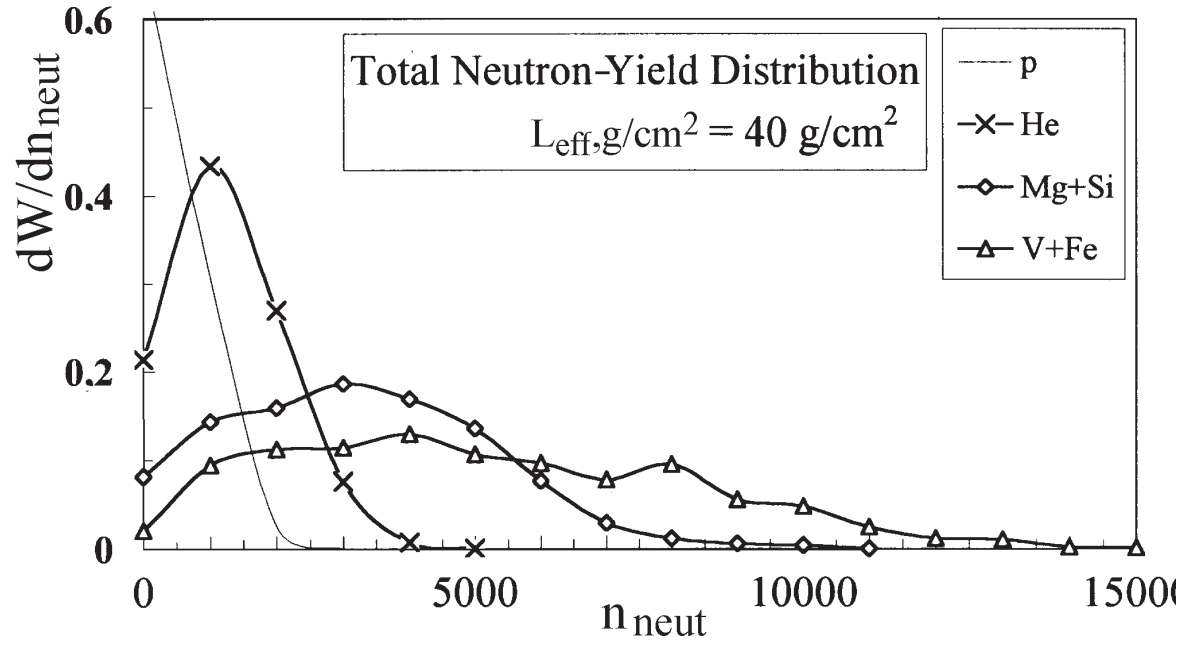

Figure 26: Distribution of the total neutron number found by integrating over the effective thickness $\Delta = 40$ g·cm^{-2} for cascades initiated by primary protons and nuclei at $E_0 = 1$ PeV.

$\pi^{\pm}, \ldots$) only almost without (or without) neutral pions. In this case, the initial cascade stage could look like a NEC initiated by a heavy nucleus, i.e., a high neutron signal and low ionization one are observed. However, the m.f.p. of primary particles seems to be sufficiently large ($\gtrsim \lambda^{p}_{int}$).

3.4 INCA's geometric factor

One of basic concepts of the INCA project is the use of light substances (e.g., polyethylene) as the dominant one of the absorber that makes it possible to provide the maximum geometry factor unattainable by another techniques. To calculate the exact value of geometric factor, the influence of event selection criteria, edge effects, equipment response functions etc. must be taken into account. It requires nice calculations and will be carried out in the course of the further project elaboration. Let us not go beyond qualitative estimates at this stage.

The INCA's geometric factor ($\Gamma = S\Omega$) is determined by 4π geometry, if we mean that the device positioned far from the Earth can detect particles traversing it in all directions. For a cube with the linear dimension $L = 2$ m, the maximum Γ value could be found by the use of the relation [57] $\Gamma'_{\max} \simeq 4\pi L^2 \simeq 48$ m^{2}sr. When demanding from the particle trajectory to traverse two cube's opposite sides, we get for these sides $\Gamma_{1/6} = \pi L^2/4$ [58], while for the cube we have $\Gamma'_{\min} = 6\,\Gamma_{1/6} \simeq 20$ m^{2}sr that is the minimum value as the above requirement is rather strong.

The angular dimension of the Earth viewed from the satellite is $\Omega_{\rm E}$. It is necessary to subtract this value from 4π. For the Earth's radius $R_{\rm E} = 6371$ km and satellite altitude $H \simeq 400$ km, $\Omega_{\rm E} = 2\pi(1 - \cos\alpha)$, where $\alpha = \arcsin\{R_{\rm E}/(R_{\rm E} + H)\}$, $C_{\rm E} = 1 - \Omega_{\rm E}/4\pi = 0.5(1 + \cos\alpha) \approx 0.67$, $\Gamma_{\rm real} = C_{\rm E}\Gamma' \simeq 13 - 32$ m^{2}sr. Let us use below the efficient value $\Gamma_{\rm eff} \simeq 20$ m^{2}sr.

As for detectors with a large umber of layers, consisting of separate long logs and registering only the ionizing component, it is necessary to exclude cases when the trajectory of particle arrival is close to the direction of a log (so called "dead" angles). If so, $\Gamma_{\rm eff}$ must be reduced by a factor $C_{\rm dead}$ which takes into account this effect and could be estimated as follows. To estimate the maximum value of "dead" angle, let us demand of the cascade axis to pass through the middles, at least, of four logs 200 cm long and 2.5 cm wide located side by side, i.e., the total shifting is l =7.5 cm. If so, for a cube's side the "dead" solid angle determined by the direction of the log is equal to $\omega_{\rm dead} \approx \pi l^2/L$. The device has four sides subject to the effect influence, however one of these sides will be periodically facing the Earth. Then the mean number of these sides is 3.3 and we have $\Omega_{\rm dead} \approx 3.3\,\omega_{\rm dead} \approx 0.93\,\pi$ $C_{\rm dead} = 1 - \Omega_{\rm dead}/4\pi \approx 0.77$.

However, the fundamental INCA property is the detection of neutrons distributed both in volume and time. In this case the situation changes fundamentally, and detection properties weakly depend on direction of primary particle arrival at all.

4 Conclusion

- A new effective techniques for direct measurements of the spectrum and mass composition of the primary cosmic rays in the "knee" range at $10^{15} - 10^{16}$ eV and the spectrum of primary electrons at $10^{11} - 10^{13}$ eV is proposed. The techniques is based on a new type device – ionization-neutron calorimeter (INCA), being very promising for future experiments in different fields of astrophysical and cosmic-ray investigations, as well as on the use and elaboration of new technologies of particle detection;

- a new effective method for measurement of cascade energy (additionally to the traditional techniques of ionization measurement) based on the detection of evaporated thermalized neutrons, which makes it possible to improve the the reliability in the range of superhigh energies, wherein large theoretical uncertainties exist.

- the use of light substances (e.g., polyethylene) as the dominant one of the absorber is proposed that makes it possible to provide the maximum geometry factor unattainable by another techniques;

- a new effective method is proposed for separation of primary electrons and protons that makes it possible to achieve a total rejection factor of $\sim 10^{-5} - 10^{-6}$ to investigate the primary electron spectrum at $E_e > 1$ TeV.

- a basically new analogue-free technology charge coordinate-sensitive detectors on the basis of semiconductor matrix bipolar silicon structures with internal amplification is specially developed for this project.

References

[1] Aleksandrov K.V., Ammosov V.V., Chechin V.A. *et al.*, The Modern Conception of the INCA Project, Nucl. Phys. B (Proc. Suppl.) (2003) 122, 427;
Chubenko A.P., Mukhamedshin R.A. *et al.*, The Modern Concept of the INCA Project, Proc. 28th ICRC, Tsukuba (2003), 2221;
Mukhamedshin R.A. *et al.*, The Russian-US INTREPID Project, Proc. 28th ICRC, Tsukuba (2003), 2225;
Aleksandrov K.V., Ammosov V.V., Chubenko A.P. *et al.* The INCA Project: Present Status and Outlook. Nucl.Phys. B (Proc. Suppl.) (2002) v. 113, 344;
Aleksandrov K.V. *et al.* A New Method of Ionization-Neutron Calorimeter for Direct Investigation of High-Energy Electrons and Primary Nuclei of Cosmic-Rays up to the "Knee" Region, Nucl. Instr. Meth. in Phys. Res. A459. (2001) 135.
Aleksandrov K.V., Ammosov V.V., Chubenko A.P. *et al.*, The INCA Collaboration: Present Status and Outlook, Proc. 27th ICRC, Hamburg (2001), V. 1, 217.
Mukhamedshin R.A. *et al.* New approach to separation of electromagnetic and hadron cascades and to energy measurement in detection of primary particles. Nucl. Phys. B (Proc. Suppl.). 2001. V. 97, p.189.
Aleksandrov K.V. *et al.*, The INCA project for direct studies of primary cosmic rays up to the "knee" energy range $10^{15} - 10^{16}$ eV. Nucl. Phys. B (Proc. Suppl.) 75A (1999) 269.
Aleksandrov K.V., Ambrosio M., Ammosov V.V. *et al.*, The INCA Project, III & IV. Proc. 26th ICRC, Salt Lake City. 1999. V. 1, pp. 219, 203 & 215.

[2] Kulikov G.V. and Khristiansen G.B., JETP 35 (1958) 635.

[3] Peters B. 1959, 6th ICRC, Moscow, (1957) vol. 3, 157

[4] Zatsepin G.T. *et al.* 1962, Izv. AN SSSR, ser. fiz., 26, 685.

[5] Ptuskin V.S. *et al.* 1993, Astron. Astrophys., 268, 726

[6] Hillas A.M., 16th ICRC, Kyoto (1979) vol. 8, 7

[7] Stamenov J.N. *et al.* 20th ICRC, Moscow (1987), 1, 410

[8] Biermann P.L. 1993, 23rd ICRC, Calgary (1993) Inv.,Rapp.,High. Papers, 45

[9] Berezhko E.G. *et al.* 1996, JETP, 82, 1

[10] Protheroe R.J., Szabo A.P. 1994, Astropart. Phys., 2, 375

[11] Nikolsky S.I. 1993, Bull.Russ. Acad. Sci., 57, 595

[12] Yakovlev V.I. Proc. 24th ICRC, Rome (1995) 1, 446

[13] Petrukhin A.A. Proc. 27th ICRC, Hamburg (2001), 5, 1768.

[14] Erlykin A.D. and Wolfendale A.W. 1997, J. Phys.G: Nucl. Part. Phys., 23, 979

[15] Erlykin A.D. and Wolfendale A.W., 1997, Astropart. Phys., 7, 1.

[16] Erlykin A.D. and Wolfendale A.W., 2001, J.Phys.G: Nucl.Part.Phys. 27, 1005.

[17] Chechin V.A. and Tsarev V.A., Proc. Russian Cosmic Ray Conf. 1998, Moscow.

[18] Chechin V.A. *et al*, Kratkie Soobsheniya po Fizike, to be published

[19] Yoshida K. *et al.*, Proc. 28th ICRC, Tsukuba (2003), 3, 1993; astro- ph/0308470

[20] Zatsepin V.I. *et al.*, Proc. 28th ICRC, Tsukuba (2003), 1829; Ahn H. S. *et al.*, ibid, 1833

[21] M.Müller *et al.*, 28th ICRC, Tsukuba (2003), 1, 101; Roth M. *et al.*, ibid, 139.

[22] Amenomori M. *et al.*, 28th ICRC, Tsukuba (2003), 1, 107; ibid, 143.

[23] J.R. Hörandel. Astropart. Phys. 19, 193 (2003).

[24] Nikolsky S.I., Stamenov J.N., and Ushev S.Z., Nucl. Phys. **B13** (1987) 883.

[25] Shen C.S., Astrophys. J. 162 (1970) L181.

[26] Kobayashi T. *et al.*, Proc. 26th ICRC, Salt Lake City (1999) V. 3, 62.

[27] Nishimura J. *et al.*, Proc. 23th ICRC, 2 (1993) 128.

[28] Atoyan A.M. *et al.*, Phys. Rev. D52(6), 1995, 3265.

[29] Nishimura J. *et al.*, Proc. 24th ICRC, Rome, 3 (1996) 29.

[30] Ashenbach B., Egger R., and Trümper J., Nature **373** (1995) 587.

[31] Erlykin A.D. and Wolfendale A.W., 2002, J.Phys.G: Nucl.Part.Phys. 28, 359.

[32] Bogdan T.J. and Volk H.J., A&A 122 (1983) 129.

[33] Heinbach U. and Simon M., ApJ, 441 (1995) 209.

[34] Fichtel C.E. *et al.*, Astron. Astrophys., 1993, vol. 97, p. 13.

[35] Bhat P.N. *et al.*, Astron. Astrophys., 1987, vol. 178, p. 242.

[36] Mayer-Hasselwander H.A. *et al.*, Proc. 23rd ICRC (Calgary), 1993, vol. 1, p. 180.

[37] Zyskin Yu. and Mukanov D., Proc. 19th ICRC (La Jolla), vol. 1, p. 177.

[38] Lominadze J.G. *et al*, Astrophys. Space. Sci., 1983, vol. 90, p. 19.

[39] Cheng K.S. *et al.*, Astrophys. J., 1986, vol. 300, p. 500.

[40] Michel F.C., Rev. Mod. Phys., 1982, vol. 54, p. 1.

[41] Sacher W. and Schonfelder V., Space Sci. Rev., 1983, vol. 36, p. 249.

[42] Acharya B.S. Ground Based γ-ray Astronomy in India. Past, Present and Future. Proc. 29th ICRC, Pune (2005). Highlight Papers.

[43] Coultre P. Cosmic Ray Observation and Results from Experiments Using LEP Detectors at CERN. Proc. 29th ICRC, Pune (2005). Highlight Papers.

[44] Stirling A. Colgate, Solar Physics, 1988, vol. 118, p. 1.

[45] Chupp E.L. *et al.*, Astrophys. J. Lett., 1982, vol. 263, p. L95.

[46] Dimopoulos S. *et al.*, Phys.Rev. D41(1990)2355.

[47] Joffe B.L *et al.*, Acta Phys. Polonica B12(1981) 229.

[48] Rujula A.de, Glashow S.L., and Uri Sarid, preprint CERN-TH.

[49] Saito T. *et al.*, Phys.Rev.Lett. 65 (1990) 2094.

[50] A.Ohsawa, E.H.Shibuya, M.Tamada. The Exotic Characteristics of Centauro-I - A model to describe Centauro-I. Proc.29th ICRC, Pune (2005).

[51] Bezrukov L.B. *et al.*, Sov.J. Nucl.Phys. 1973, 17 98.

[52] Britvich G.I. *et al.*, Instr. & Experimental Techniques 45/5 (2002), 644.

[53] Fedorova G.F. and Mukhamedshin R.A. Bull. Soc. Sci. Lettr. Lodz, Ser. Rech. Def. 1994. V. XVI, p.137.

[54] Shabelsky Yu., Zh.Phys.C **38** (1988), no. 4, 569.

[55] Dementyev A.V. and Sobolevsky N.M. SHIELD - Universal Monte Carlo Hadron Transport Code. Proc. 3rd Workshop on Simul. Accelerator Radiation Environments (SARE3), KEK, Tsukuba (1997). KEK Proc. 97-5, Ed. H.Hirayama, p.21.

[56] Dementyev A.V., Sobolevsky N.M., and Stavissky Yu.Ya. Nucl. Instr. and Meth., A374 (1996) 70.

[57] Grigorov N.L. and Tolstaya E.D., Proc. 27th ICRC, Hamburg (2001) 2329;
Grigorov N.L. Space Research (1997) V.35, 339 (in Russian)

[58] Murzin V.S. Introduction into cosmic ray physics. M.: Atomizdat, 1979 (in Russian).